

1N-20
200653
76 p

NASA Contractor Report 191204

A Study of DC-DC Converters With MCT's for Arcjet Power Supplies

Thomas A. Stuart
University of Toledo
Toledo, Ohio

January 1994

Prepared for
Lewis Research Center
Under Grant NAG3-1102



(NASA-CR-191204) A STUDY OF DC-DC
CONVERTERS WITH MCT'S FOR ARCJET
POWER SUPPLIES Final Report
(Toledo Univ.) 76 p

N94-27662

Unclas

G3
20/20 0206653

Table of Contents

	<u>Page</u>
I. INTRODUCTION	1
A. MCTs vs. FETs	2
B. Resonant vs. Soft Switching Converters	3
C. Series Resonant Converters	5
II. POWER CIRCUIT OF THE 10-KW ARCJET POWER CONVERTER	9
A. Series Resonant Converter (SRC) Description	9
B. Design of SRC	17
III. POWER CIRCUIT PERFORMANCE AND EXPERIMENTAL DATA	37
A. Power Circuit Description	37
B. Steady-State Performance	42
C. Load Transient Tests	51
IV. IGNITION CIRCUIT.....	59
A. Power Circuit Design.....	59
B. Experimental Results	64
V. SUMMARY.....	73
REFERENCES.....	74

Abstract

A Study of DC-DC Converters with MCT's for Arcjet Power Supplies

by

Thomas A. Stuart

Many arcjet DC power supplies use PWM full bridge converters with large arrays of parallel FETs. This report investigates an alternative supply using a variable frequency series resonant converter with small arrays of parallel MCTs. The reasons for this approach are to: 1) Increase reliability by reducing the number of switching devices; 2) Decrease the surface mounting area of the switching arrays. The variable frequency series resonant approach is used because the relatively slow switching speed of the MCT precludes the use of PWM. The 10kW converter operated satisfactorily with an efficiency of over 91%. Test results indicate this efficiency could be increased further by additional optimization of the series resonant inductor.

I. INTRODUCTION

Many of the present DC power supplies for arc jet thrusters utilize a full bridge DC-DC converter similar to those in [1-3]. These circuits employ four switches that usually consist of multiple FETs connected in parallel, and phase shift control is used to regulate the output. The operating frequency is usually limited to the 10-20 kHz range where switching loss is very low because of the fast switching times of the FETs. Higher frequencies have been avoided because large ferrite transformer cores have not been considered satisfactory for a spacecraft environment. Most of these converters have been intended for lower power applications (e.g., 1-2 kW) which are supplied from a 28 Vdc source. At this voltage, no other switching device is capable of providing the efficiency and cost effectiveness of FETs.

However, for higher power levels such as 10 kW, it becomes desirable to increase the source voltage to 150 - 300 Vdc in order to avoid the exceptionally high currents that would accompany a 28 Vdc source. At this higher voltage level, other switching devices such as the IGBT and the MCT become competitive with the FET. This is because the forward voltage drop of the FET climbs rapidly for breakdown voltages above 200 volts, and a very large number of devices must be operated in parallel to achieve the forward drop of an IGBT or an MCT. If the application is not cost sensitive, it is still feasible to operate FETs in this manner, but very large arrays of FETs are required. This is especially true when attempting to match the forward drop of an MCT, which promises to have a much lower forward drop than an IGBT with the same die size [4]. Because MCTs offer the prospect of a large reduction in the number of switching devices, it was decided to investigate the use of these devices in a 10 kW arcjet power supply.

A. MCTs vs. FETs

The MCT module described in [4] consisted of 6 parallel die and had a nominal current rating of 300 amps. This device was a prototype MCT power module developed by the General Electric Corporate Research and Development Center.

A 10 kW converter with an input voltage of 150 Vdc (specified input voltage when research proposal was submitted) and an efficiency of 90% will draw an average input current of 74 Adc. At 74 amps and $T_J = 125^\circ\text{C}$, the GE MCT has a forward drop of about 0.75 volts. No breakdown voltage ratings were given in [4] for this device, but it is presumed to be about 600 volts since it was operated from a 270 Vdc bus and compared with a 600 volt IGBT.

To achieve this same drop at 74 amps with FETs, one might consider the IRFK4H450 module, which has an $R_{\text{dson}} = 0.19 \Omega$ at $T_J = 125^\circ\text{C}$ and consists of 4 parallel die. This device has a peak voltage rating of 500 volts. To get a drop of .75 V. @ 74 A would require 19 parallel modules, or 76 parallel die. This means that a full bridge converter would need a total of $4 \times 76 = 304$ die. While it is feasible to construct such a circuit, it should be remembered that a short circuit failure of any single die will destroy the entire power supply unless each die has an individual fuse. Packaging restrictions may be another problem, and the drive circuits will need a high impulse current capability because of the high input capacitance of the FET arrays. All of these problems would be greatly alleviated by using MCTs, since a circuit with the same forward drop would contain only $6 \times 4 = 24$ die.

MCTs are much slower than FETs however, so the MCT would not be competitive in a conventional 20 kHz phase shift circuit because of its higher switching loss. The GE MCT in [4], for example, has a current fall time of 1714 n.s. as compared to 70 n.s. for the IRFK4H450. Therefore the MCT would have to

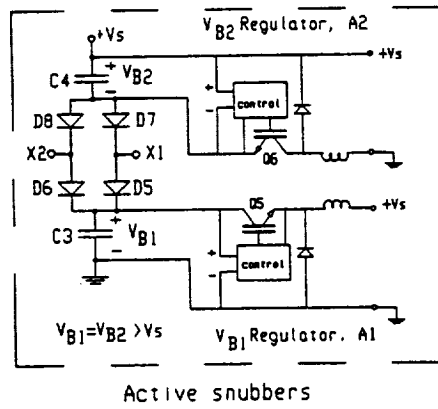
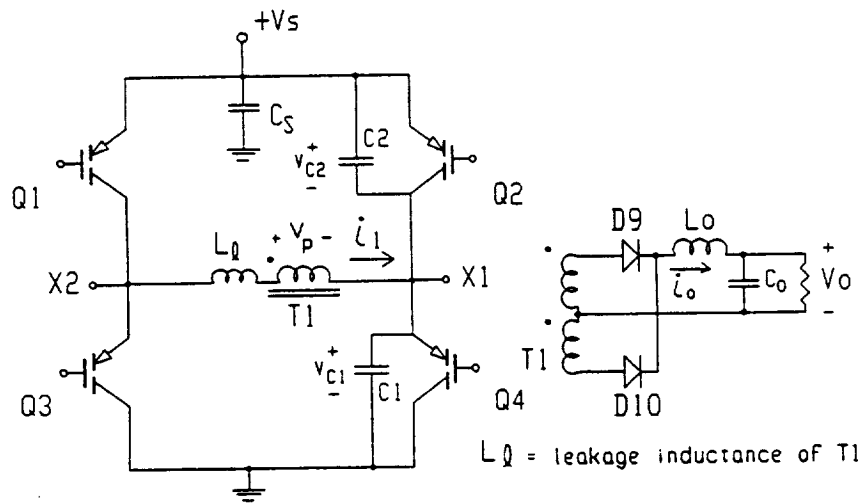
be used in some type of resonant or soft switching circuit where switching losses are reduced.

B. Resonant vs. Soft Switching Converters

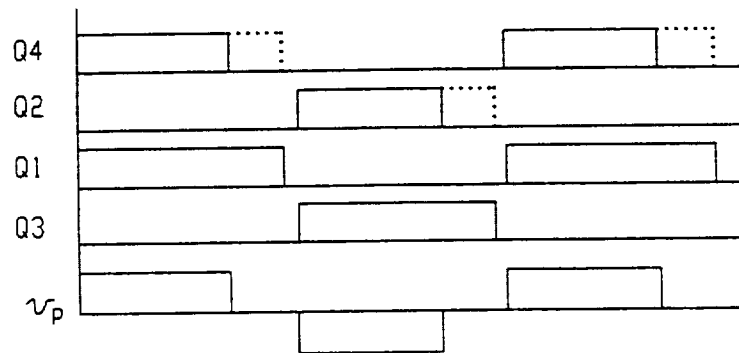
When this project was first initiated, it appeared that one of the better candidate circuits might be the ZVS/ZCS (zero voltage switching, zero current switching) converter shown in Fig. I-1. Earlier versions of this circuit are described in [3, 5-8]. These earlier circuits are satisfactory for power levels in the 1-2 kW range, but they are difficult to implement at higher power levels. The more recent version in Fig. I-1 overcomes this limitation by using an active snubber which recycles part of the energy back to the source. To date, a 10 kW 20 kHz version of the circuit has achieved an efficiency of 91.3%, even with high voltage drop IGBTs and a relatively low output voltage of 36 Vdc [9].

As seen from the timing diagram in Fig. I-1, on a typical half cycle for Q1 and Q4, both devices turn on simultaneously, but Q4 turns off first. When Q4 turns off, C1 provides a path for the load current and v_{C1} rises at a gradual rate. Thus C1 provides zero voltage switching (ZVS) for Q4. Assuming Q2 has reverse blocking capability, v_{C1} continues to increase beyond V_s , but when $v_{C1} = V_{B1}$, D5 conducts and v_{C1} is clamped at this value. Since $V_{B1} \gg V_s$, i_1 is rapidly driven to zero, and zero current switching (ZCS) is achieved for Q1 since $i_1 = 0$ before Q1 is turned off. After i_1 reaches zero, a very slight reverse current flows through Q1 before it recovers. D6 is required to clamp the voltage across Q3 when Q1 recovers.

Although the circuit in Fig. I-1 has proven to be advantageous for higher input voltages, two developments occurred which indicated that it probably would not be competitive for the present application. First of all, the input voltage specification decreased from 150 to 120 Vdc, and there was some indication that it might drop even further. The second was that the available MCTs had lower than anticipated reverse breakdown voltages, and this would have required the use of



(a.) Power circuit with active snubbers.



(b.) timing diagram for gate drivers.

Fig I-1. ZVS/ZCS converter with MCT's

series blocking diodes D1-4, as shown in Fig. I-2. The lower input voltage plus the extra drop of the diodes indicated that the ZVS/ZCS probably would have an excessive conduction loss as compared to other topologies. Therefore, it was decided to use the conventional series resonant circuit in Fig. I-3 instead of the ZVS/ZCS.

C. Series Resonant Converters

The series resonant circuit (SRC) in Fig. I-3 is well known in the power electronics community, and it has been analyzed extensively [10-17]. If slower devices such as IGBTs or MCTs are used for Q1-Q4, the circuit should be controlled by varying the frequency (instead of PWM) in order to reduce the turn-off switching losses. D5 and D6 also have very low turn-off loss, but D1-D4 still have significant turn-off loss. All of the conduction losses will be higher than for conventional phase shift PWM because the current has a higher RMS/average ratio. This indicates an increased disadvantage for FETs in this circuit because of their I^2R loss characteristic. In spite of the advantages for Q1-Q4 and D5-D6, it also should be noted that the higher AC currents are a disadvantage for all of the power level capacitors and magnetics because of their higher losses.

Although the SRC exhibits higher conduction losses, the 15 kHz MCT version achieved an efficiency of 91% at 10 kW. However, it should be noted that this was accomplished only after an extensive re-design of T1 and L_r , and the temperature rise of L_r in particular was still higher than expected. This proved to be the case even when foil conductors or cables with #22 magnet wire were used (although the individual strands in this cable were insulated, it would not be proper to call this a Litz cable since the strands were not interwoven). Since these conductors appear to be satisfactory for the skin depth at 15 kHz, the excessive heating appears to be related to proximity effect losses and possibly heat transfer problems associated with larger cables. These heating problems did not appear to be caused

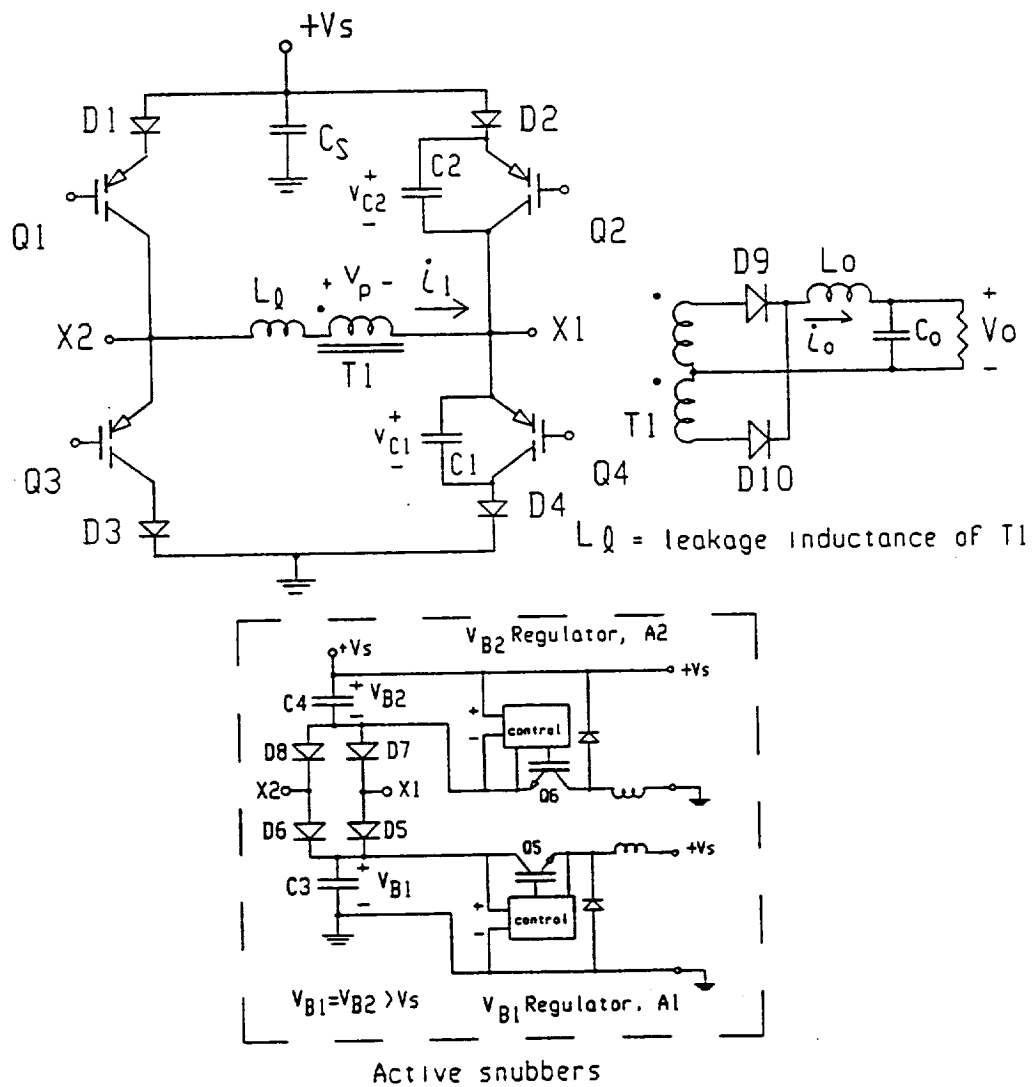


Fig I-2. ZVS/ZCS converter with MCT's and blocking diodes.

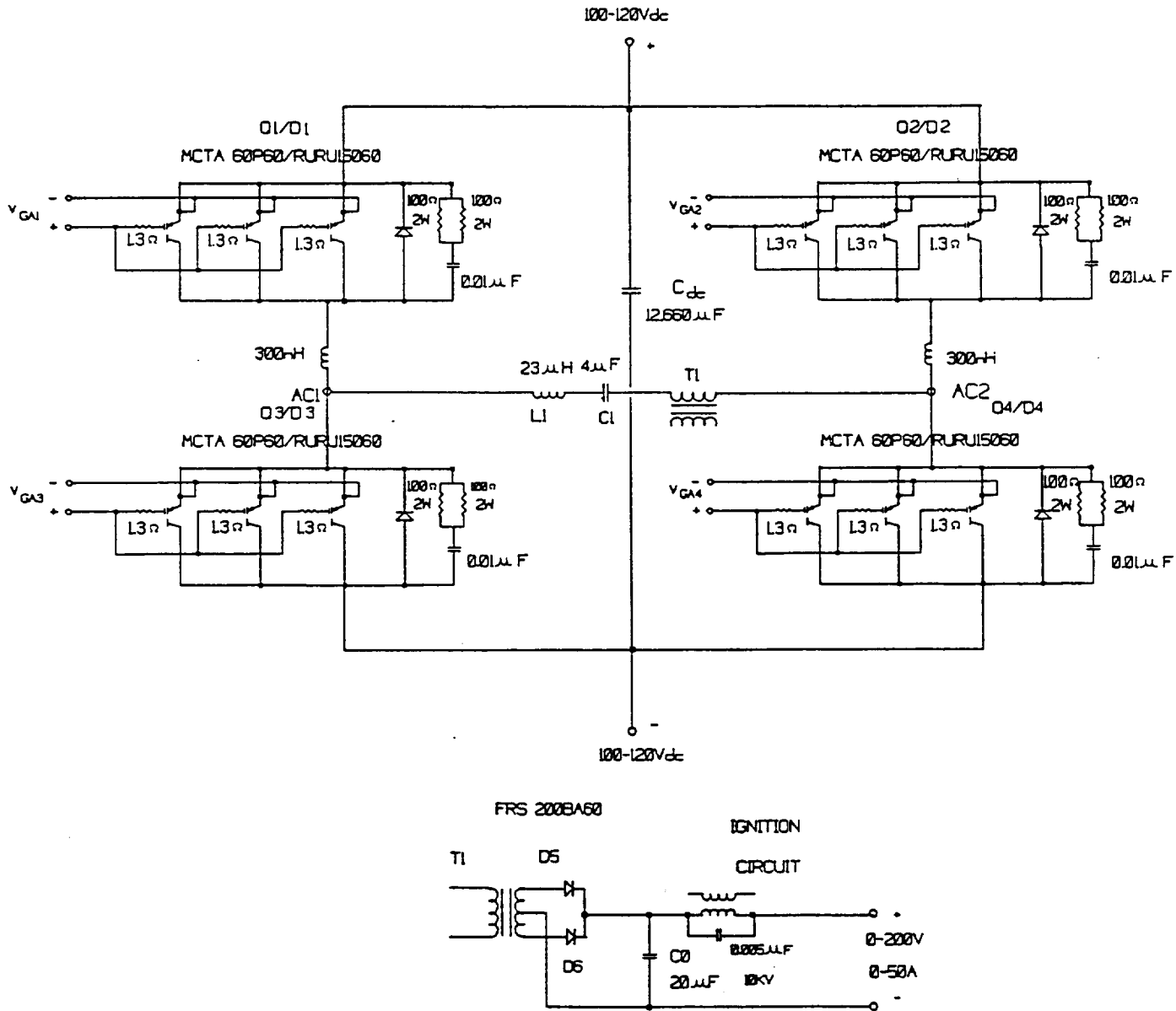


Fig I-3 Series resonant converter with MCTs.

by core losses however, since all calculations indicated that these should have remained well below the acceptable range. The final L_r design operated satisfactorily, but this was achieved only after resorting to a three-turn three-layer winding. Naturally, this also produced a core that was larger than desirable. It appears the subjects of proximity effect losses and heat transfer for magnetic components in this power range deserve further attention, and additional research in this area is certainly warranted.

II. POWER CIRCUIT OF THE 10-KW ARCJET POWER CONVERTER

A. Series Resonant Converter (SRC) Description

Fig. II-1 shows the schematic of the SRC power circuit which was developed for this study. The variable frequency control circuit is shown in Fig. II-2, while the gate pulse logic is shown in Fig. II-3. The gate drivers for the MCTs are shown in Fig. II-4.

Since this converter is intended to power an arcjet thruster, it is designed to operate as a current regulator. A voltage limit loop is also required to prevent an excessive output voltage under light loading conditions. Variable frequency control is provided by the LM 566 voltage controlled oscillator (VCO) in Fig. II-2. The current regulation loop is controlled by the circuitry associated with op amps A1 and A2, while the voltage limit loop is controlled by the circuitry associated with A3.

The gate drive logic in Fig. II-3 can be explained with the aid of the waveforms in Fig. II-5. Fig. II-5 (a.) represents continuous current operation, while Fig. II-5 (b.) shows the discontinuous mode. Referring to Fig. 5 (a), as the switching frequency approaches the resonance frequency, it becomes necessary to decrease the width of the Q14 and Q23 drive signals while maintaining a constant deadtime, t_{δ} . However, in the discontinuous mode represented in Fig. II-5 (b.), Q14 and Q23 should be limited to some value, t_n , to avoid re-triggering the same switches at the end of each half cycle. The maximum t_n is determined by the upper one-shot, while the minimum t_{δ} is determined by the lower one-shot.

The isolated gate driver used with the MCTs is shown in Fig. II-4. A discrete design was used for this gate driver to allow increased flexibility over the available integrated gate drivers. It should be noted that the MCTs require a negative gate-anode voltage (the MCT is characterized on its data sheet with -10 V) for turn on. The manufacture recommends a positive gate-anode voltage (the MCT is

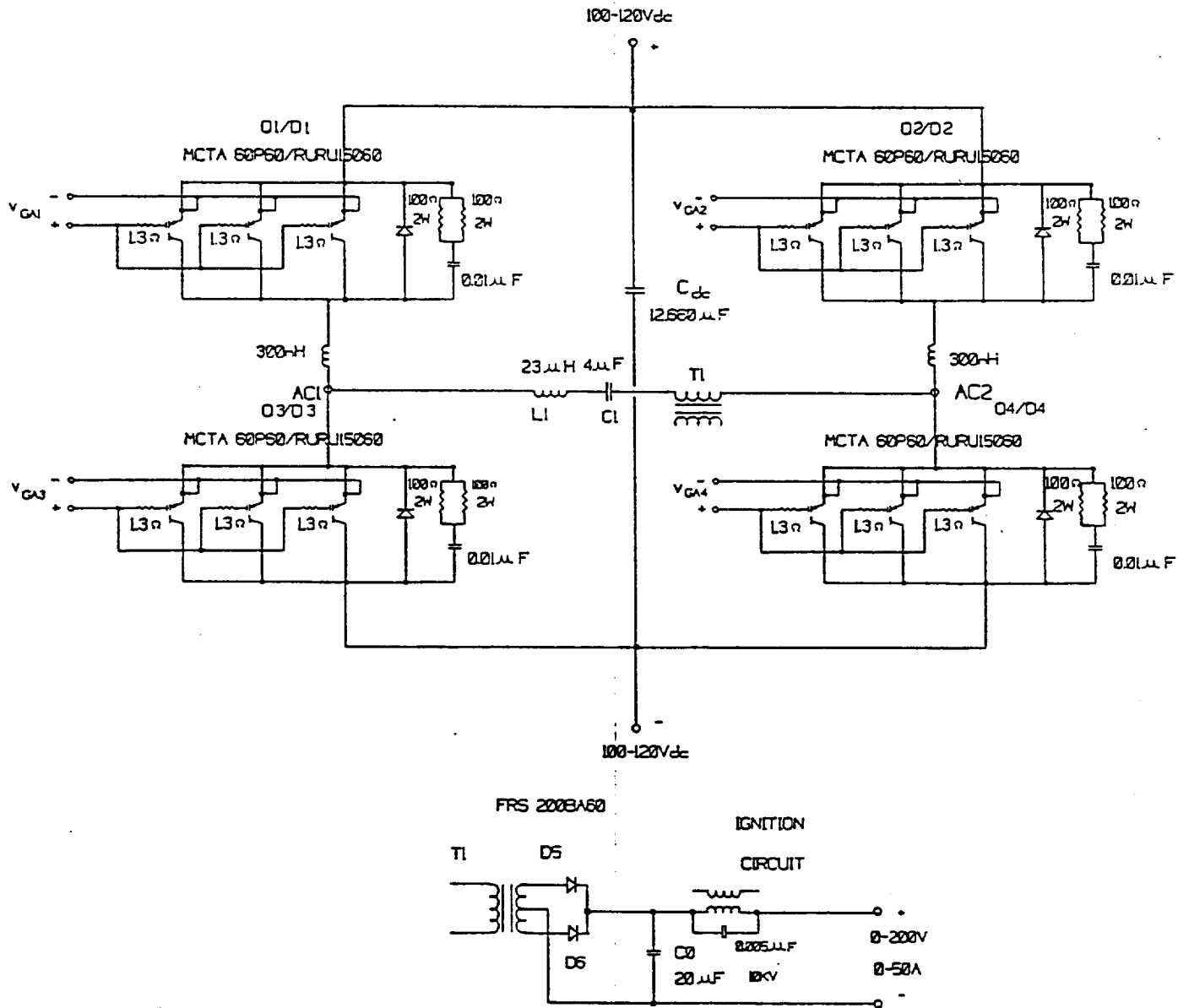
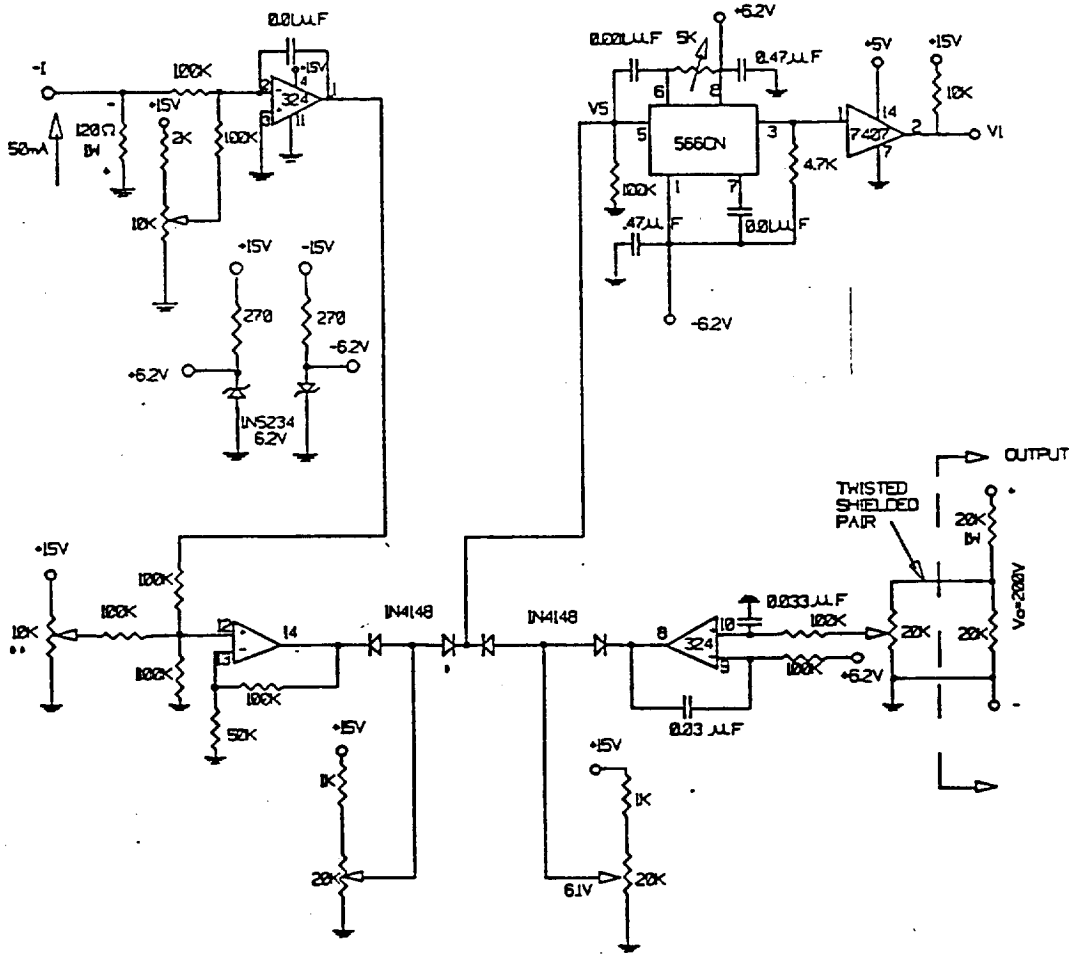


Fig II-1 Power circuit of 10-kW, 100-120V arcjet power converter.



*Prevents Parasitic Osc.
 **Sets $4.5 < V_5 < 6.1$

$$f_o = \frac{2(V-V_5)}{RICIV}$$

Fig II-2 Variable frequency control circuit for SRC.

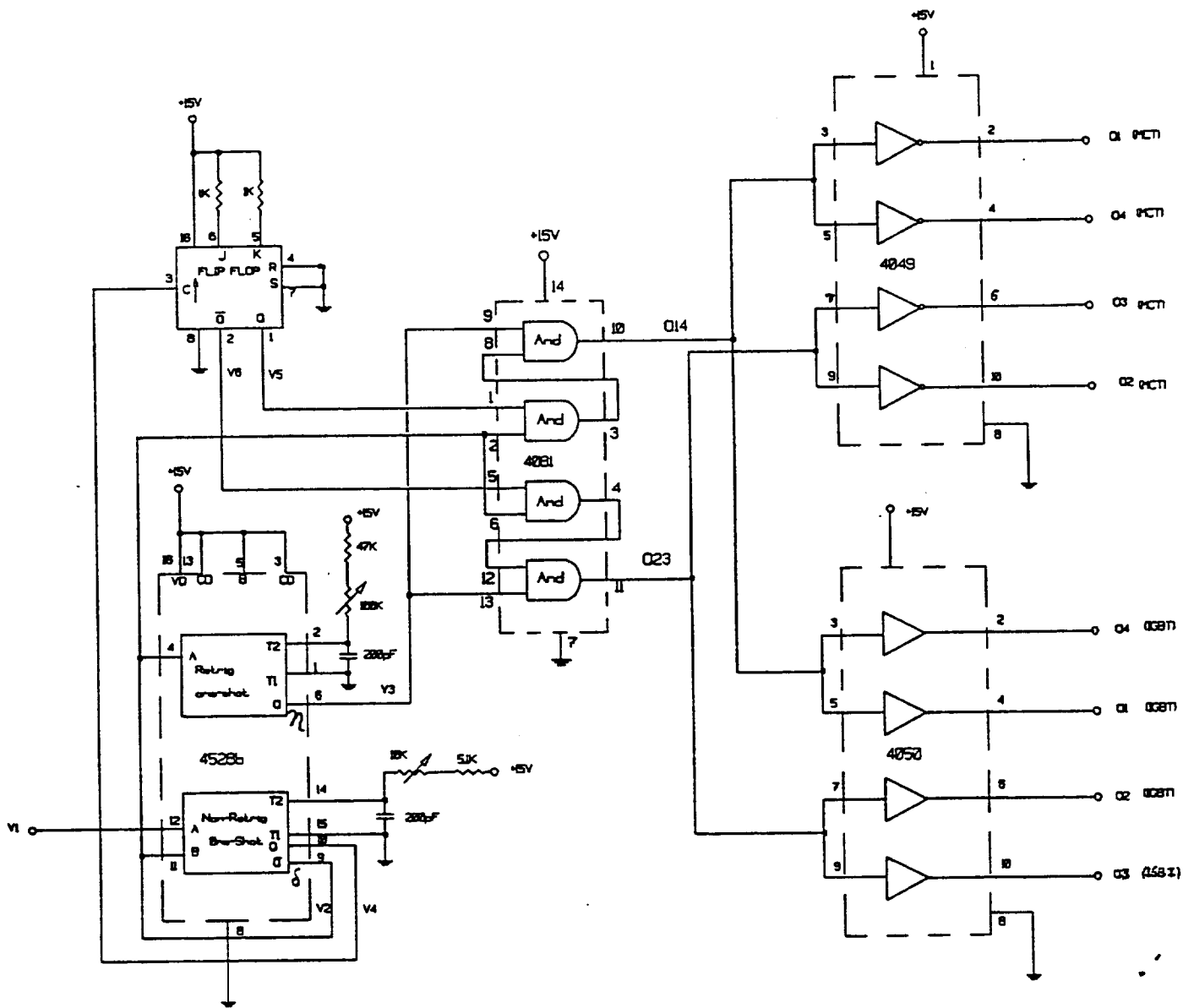


Fig II-3 . Gate pulse logic for SRC.

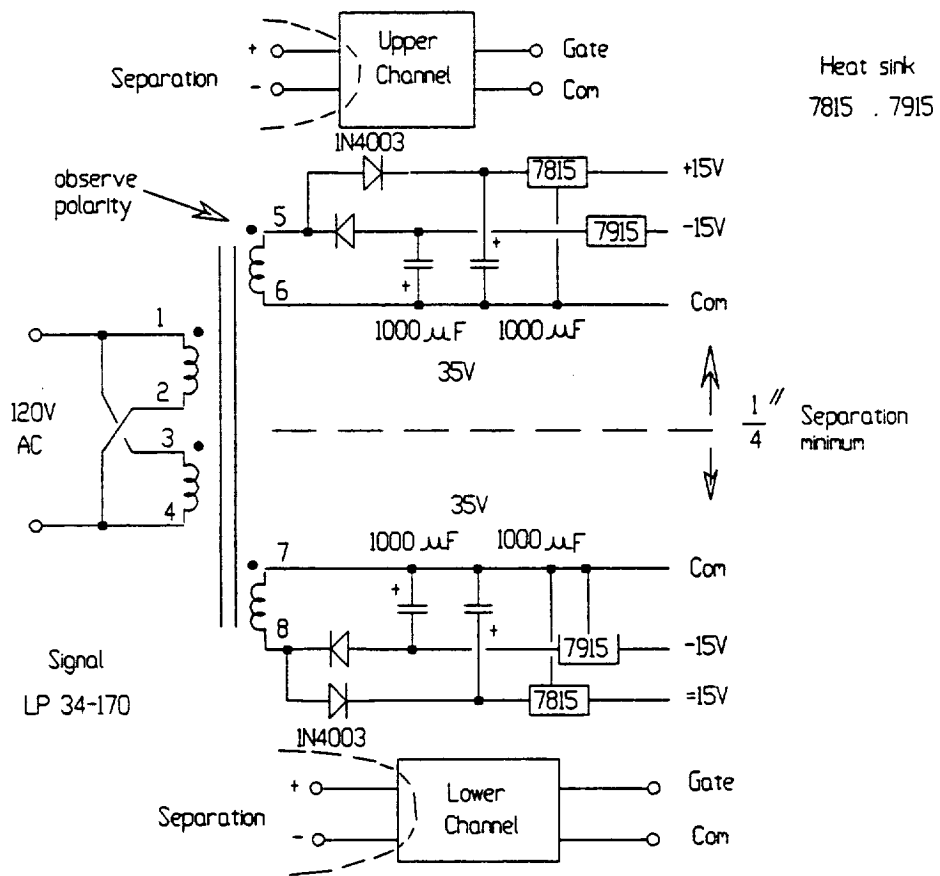
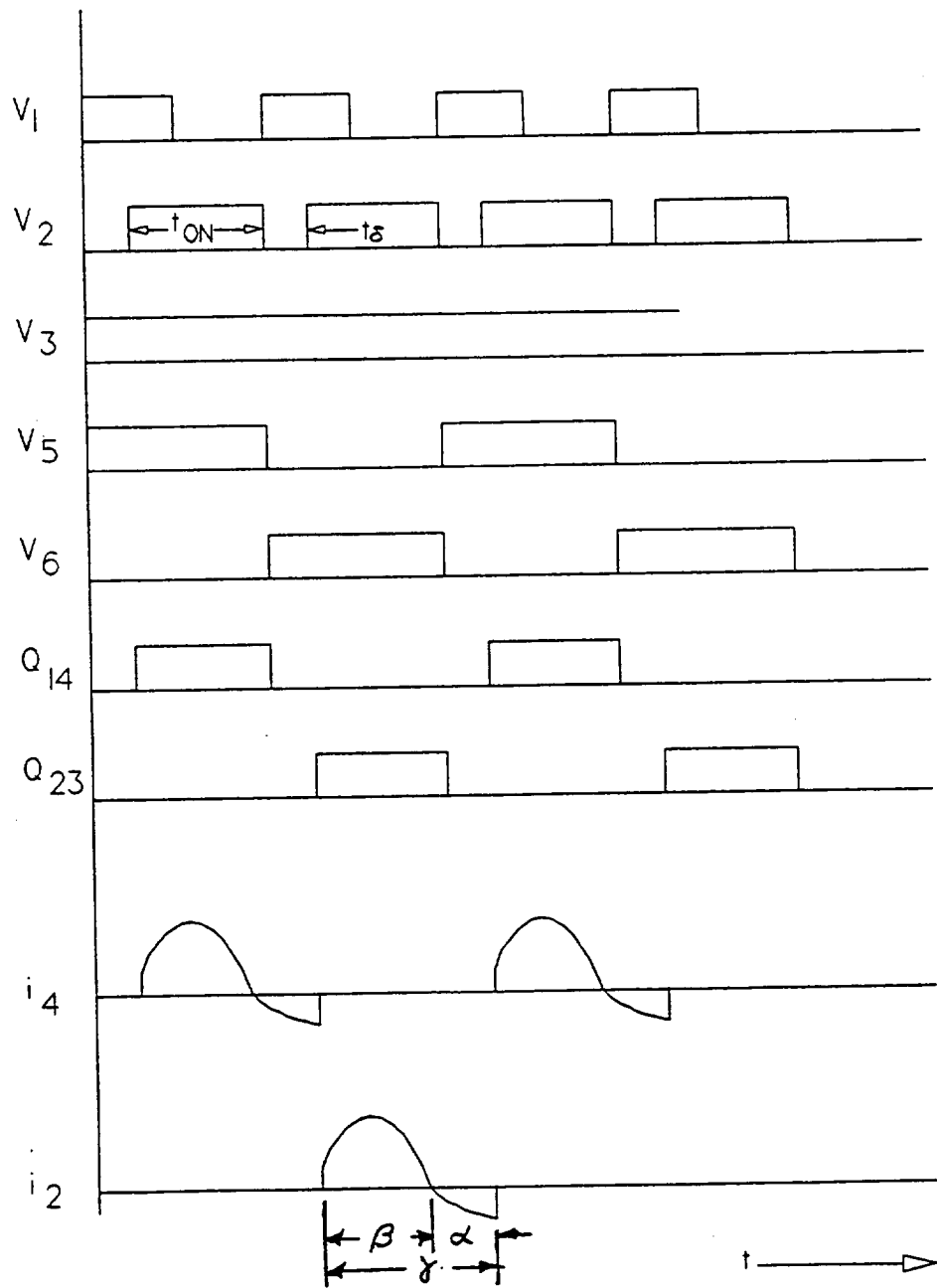
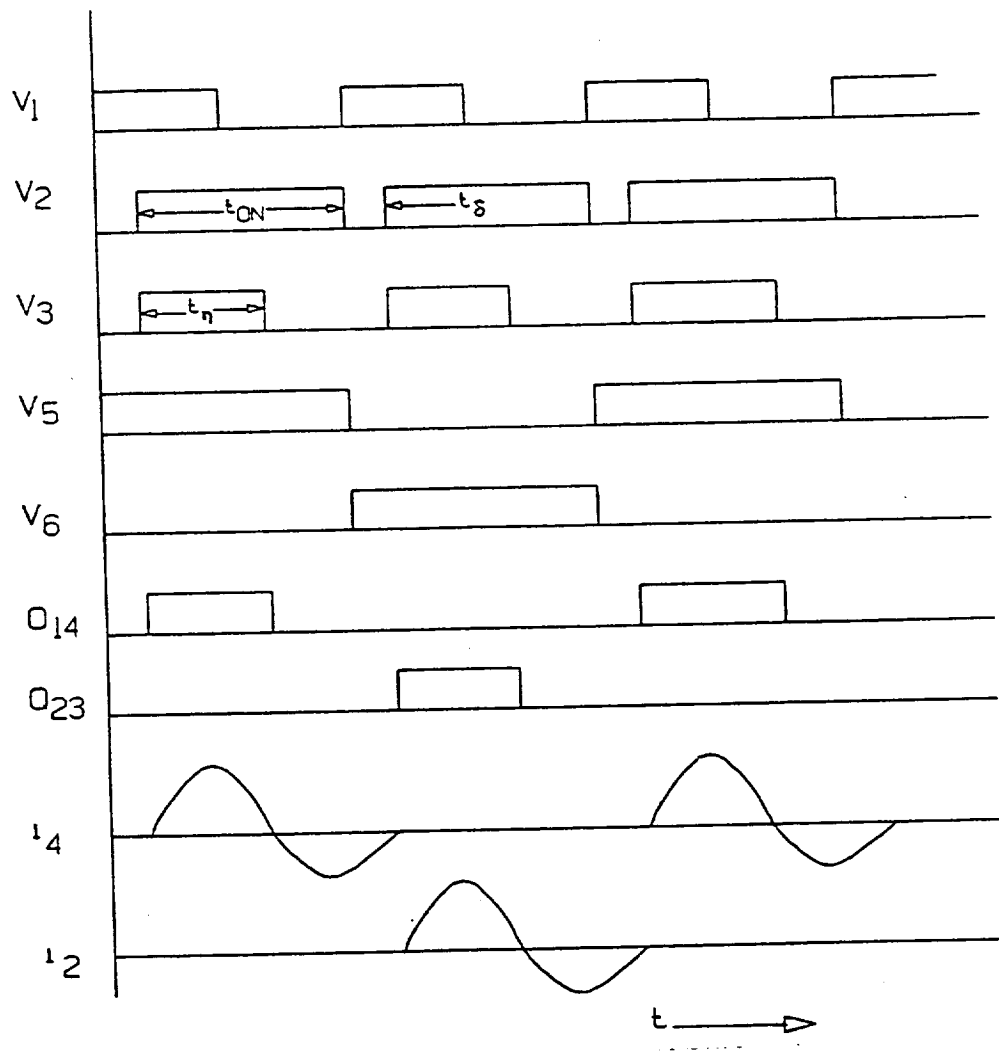


Fig. II-4(b) Isolated power supply for two channels of the MCT gate driver.



(a) Continuous operation

Fig II-5 Logic timing diagram



(b) Discontinuous operation

Fig II-5 Logic timing diagram (cont.)

characterized with +15 V) to ensure turn off. Voltages of + and -15 V were used in the gate driver with good results (the MCT maximum gate-anode voltage is 20 V). Isolated gate drive is supplied by a low-capacitance 60-Hz transformer; the gate signals are transferred through a high speed opto-isolator (HP2602). The problem of coordinating the application of gate drive signals and the anode voltage to the MCTs was not addressed in this gate driver. However, this is an issue which would affect the reliable use of MCTs, because the MCT cannot be assumed to be off with zero gate voltage.

B. Design of SRC

Fig. II-7 shows plots of the normalized continuous load current, I_{AN} , vs. the diode conduction angle, α , for various ratios of q , where q is the ratio of the reflected output voltage to the input voltage. These curves are based on the following equations which are derived in [14],

$$I_{AN} = \frac{2(1+q)(1-\cos\alpha)}{(\alpha+\beta)(q-\cos\alpha)} \quad (\text{II-1})$$

where $q = \frac{nV_o}{V}$

n = primary to secondary ratio
of T1 in Fig. I-3.

α = diode conduction angle in Fig. II-5 (a)

β = MCT conduction angle in Fig. II-5 (a), which can be found from (II-3)
below

α (also called the delay angle) is the independent variable which is varied to control I_{AN} . Actually this is done indirectly since the controller actually varies the angle, γ , where,

$$\gamma = \alpha + \beta \quad (\text{II-2})$$

Since β is a function of α (see II-3 below), controlling γ also controls α .

For continuous current,

$$\beta = \pi + \tan^{-1} \left[\frac{(q^2 - 1) \sin \alpha}{2q - (1 + q^2) \cos \alpha} \right] \quad \text{rad} \quad (\text{II-3})$$

To find the actual average current, I_{avg} , use the equation,

$$I_{avg} = I_{AN} \times I_B \quad \text{Amps} \quad (\text{II-4})$$

where $I_B = \text{base current} = \frac{V_s}{Z} \text{ Amps}$

$$Z = \sqrt{\frac{L_r}{C_r}} \quad \Omega$$

In this case,

$$V_s = 120 \text{ Vdc} \pm 10\% (108-132 \text{ Vdc})$$

Assume a range of 104 - 128 Vdc due to series voltage drops. Also assume,

$$q = 0.9$$

Therefore, @ low line, reflected $V_o = .9 \times 104 \cong 94 \text{ V}$.

Assume,

$$V_{sec.} \cong 200 + 2.4 = 202.4 \text{ V.}$$

$$(2.4 \text{ V.} \cong \text{series voltage drop on secondary})$$

$$\therefore n = \frac{94}{202.4} = .46$$

Assuming an efficiency of 90%,

$$P_{IN} = \frac{10 \text{ kW}}{.9} = 11.1 \text{ kW}$$

Therefore,

$$I_{avg} = \frac{11.1 \text{ kW}}{104 \text{ V.}} = 107 \text{ Adc}$$

From Fig. II-7 for $\alpha = 35^\circ$ and $q = .9$ we get,

$$I_{AN} \cong 2.5$$

Therefore,

$$I_B = \frac{I_{avg}}{I_{AN}} = \frac{107}{2.5} = 42.8A.$$

$$Z_o = \frac{V_S}{I_B} = \frac{104}{42.8} = 2.43\Omega$$

Therefore,

$$\frac{L_r}{C_r} = (2.43)^2 = 5.9$$

We can now derive the following relationships between the switching frequency, f_s , and the natural resonance frequency, f_o . From Fig. II-5(a) for continuous current,

$$2\gamma = \omega_o T_s \tag{II-5}$$

$$\text{where } T_s = 1/f_s$$

$$\omega_o = \frac{1}{\sqrt{L_r C_r}}$$

Therefore,

$$\omega_o = 2\gamma f_s \tag{II-6}$$

$$\text{or } f_o = \frac{\gamma}{\pi} f_s \tag{II-7}$$

Equations (II-2) and (II-3) can be used to plot γ vs. α for various q as in Fig. II-6.

From Fig. II-6 for $q = .9$ and $\alpha = 35^\circ$ we get,

$$\gamma \cong 196^\circ$$

Therefore,

$$f_o = \frac{196}{180} f_s = \frac{196}{180} \times 15 \times 10^3 = 16.33 \text{ kHz}$$

$$\omega_o = 2\pi f_o = 102.6 \times 10^3 \text{ rad.} = \frac{1}{\sqrt{L_r C_r}}$$

Therefore,

$$L_r C_r = 94.95 \times 10^{-12}$$

and since $\frac{L_r}{C_r} = 5.9$,

we get

$$C_T = 4\mu\text{fd}$$

$$L_T = 23.7\mu\text{H}$$

We can now calculate several other important parameters for the circuit. Figs. II-8 through II-12 show the following normalized variables as functions of q and α . These curves are all based on equations derived in [14]. The base current, I_B , was previously defined and,

$$V_B = \text{base voltage} = V_s$$

$$\text{normalized RMS current} = I_{RN} \quad (\text{Fig. II-8})$$

$$\text{normalized peak current} = I_{PN} \quad (\text{Fig. II-9})$$

$$\text{normalized avg. MCT current} = I_{QN} \quad (\text{Fig. II-10})$$

$$\text{normalized avg. diode current} = I_{DN} \quad (\text{Fig. II-11})$$

$$\text{normalized peak capacitor voltage} = V_{PN} \quad (\text{Fig. II-12})$$

For $q = .9$ and $\alpha = 35^\circ$ min., we obtain the following values.

$$I_{RN} = 2.75 \quad , \quad I_{RMS} = 117.7 \text{ A. rms}$$

$$I_{pN} = 4.15 \quad , \quad I_{\text{peak}} = 177.6 \text{ A. peak}$$

$$I_{QN} = 1.125 \quad , \quad I_{Q\text{avg}} = 48.2 \text{ A. avg}$$

$$I_{DN} = .0625 \quad , \quad I_{D\text{avg}} = 2.7 \text{ A. avg}$$

$$V_{pN} = 4.15 \quad , \quad V_{C\text{peak}} = 431.6 \text{ V. pk.}$$

However, it should be noted that the above data does not represent the maximum values for all variables. This is illustrated by Figs. II-13 through II-18 where the track of α is plotted as q approaches 0.1 (the lowest value plotted) while I_{avg} is held constant. These values are obtained by plotting the α track for constant I_{AN} in Fig. II-13 and then using each pair of q and α values to find the corresponding track on Figs. II-14 through II-18. The I_{RN} , I_{PN} and I_{QN} tracks either remain fairly flat or decrease in value, but I_{DN} and V_{PN} both increase to produce the following maximum values at $q = 0.1$,

$$I_{DN_{max}} = .563 \quad , \quad I_{D_{max}} = 24.1 \text{ A. avg.}$$

$$V_{PN_{max}} = 4.7 \quad , \quad V_{CP_{max}} = 488.8 \text{ V. pk}$$

To determine the AC ripple currents for C_s and C_o we use,

$$I_{rms} = \left[I_{avg}^2 + \sum_{n=1}^{\infty} I_n^2 \right]^{1/2}$$

where I_n = RMS value of the nth harmonic

Therefore for C_s ,

$$\begin{aligned} I_{cs} &= \left[I_{rms}^2 - I_{avg}^2 \right]^{1/2} \\ &= \left[(117.7)^2 - (107)^2 \right]^{1/2} \\ &= 49 \text{ A. rms.} \end{aligned}$$

The actual transformer used a turns ratio $n = .412$, so for C_o ,

$$I_{co} = 20.2 \text{ A. rms.}$$

These ripple currents are well within the ratings of polypropylene capacitors, but if electrolytics are used to provide lower ripple voltages, the current rating usually determines the capacitor size instead of the filtering requirements. This particular design used an electrolytic and polypropylene combination for C_s and polypropylene only for C_o .

The RMS load current values did not pose a particular problem for C_r , but it was necessary to use higher voltage SCR commutation type capacitors to achieve the necessary voltage ratings.

It was originally thought that the 23.7 μH inductor could be implemented simply by increasing the leakage inductance of T1, which would eliminate one of the larger components. This was done using two ferrite "C" cores with the primary wound on one leg of the core. The secondary was then divided, with part of the winding on top of the primary and the remaining part on the opposite core leg. The two parts were divided experimentally to achieve a leakage close to 23.7

μH . The resulting circuit performed well at smaller loads, but as the load approach 4-5 kW, the conduction losses became excessive and the efficiency was only about 80%. This heating appears to have been caused by eddy currents in the windings induced by the leakage flux and/or proximity effects.

T1 and L_r were then separated, and it was determined that it was necessary to limit the number of turns on each of these devices and to limit the number of winding layers. Various gapped core and winding combinations were evaluated for L_r , but the only one that was considered successful was a design that used only 3 turns on a rather large ferrite core. This inductor is discussed in greater detail in a following section.

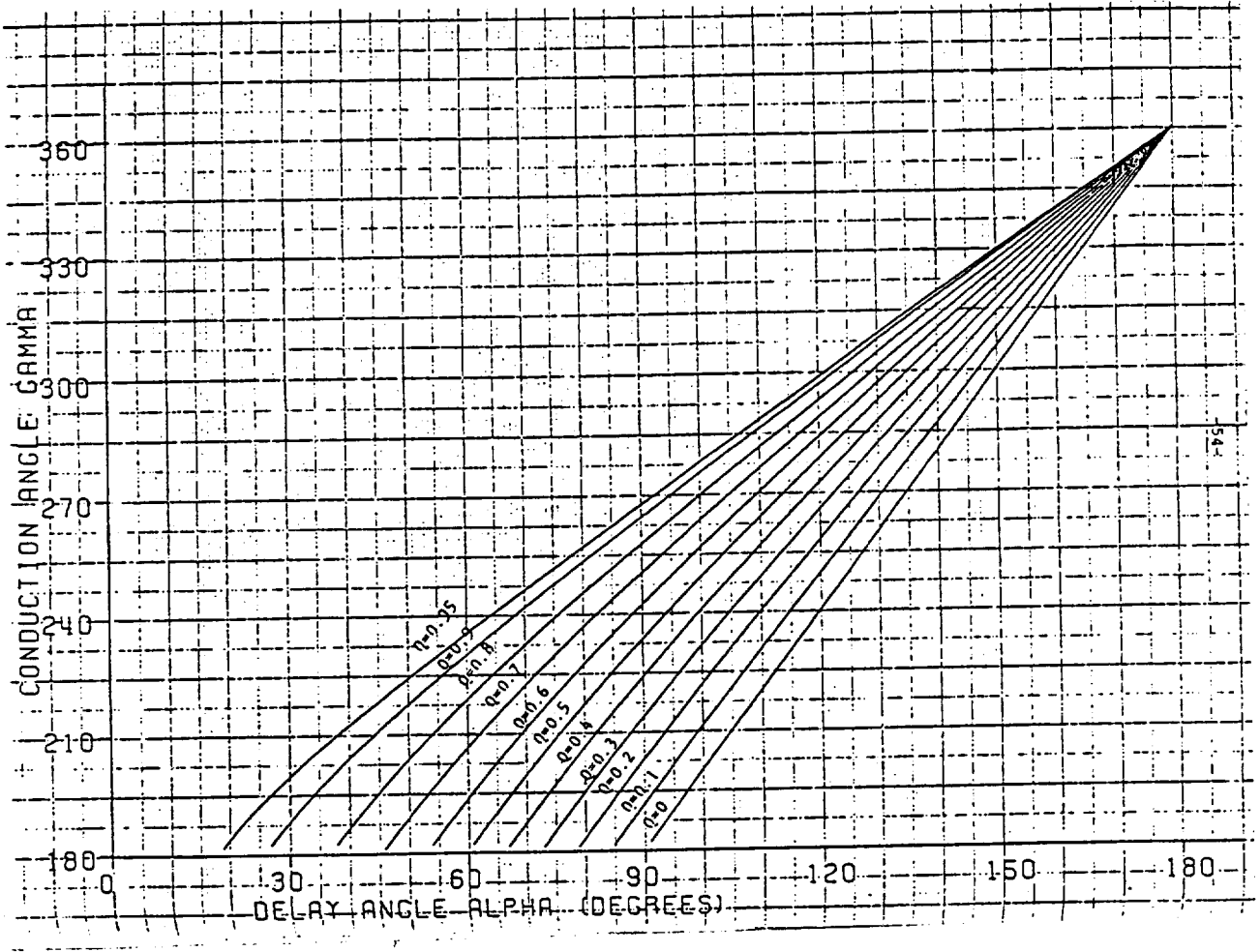


Fig II-6. γ vs α

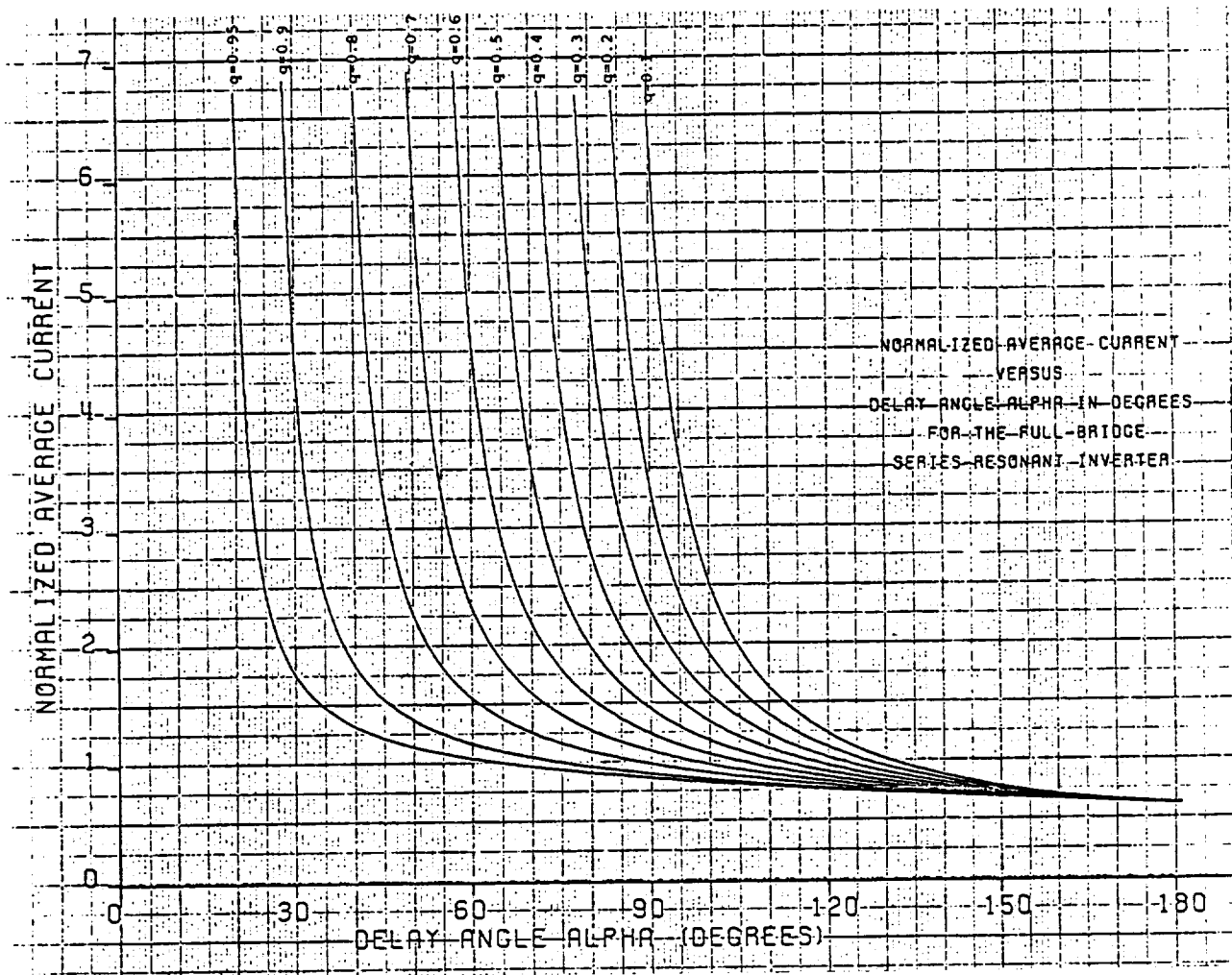


Fig II-7. I_{AN} vs α

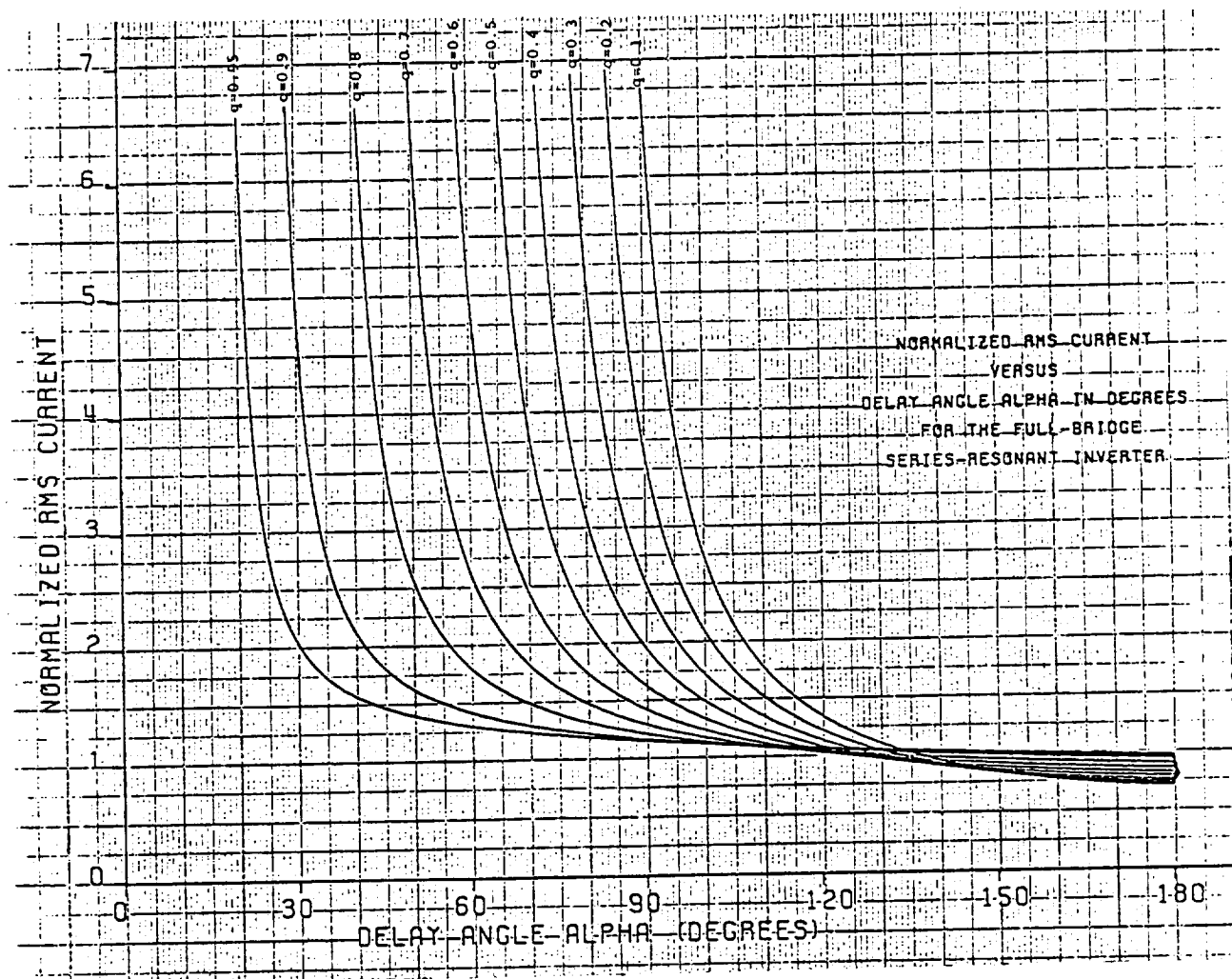


Fig II-8. I_{RN} vs α

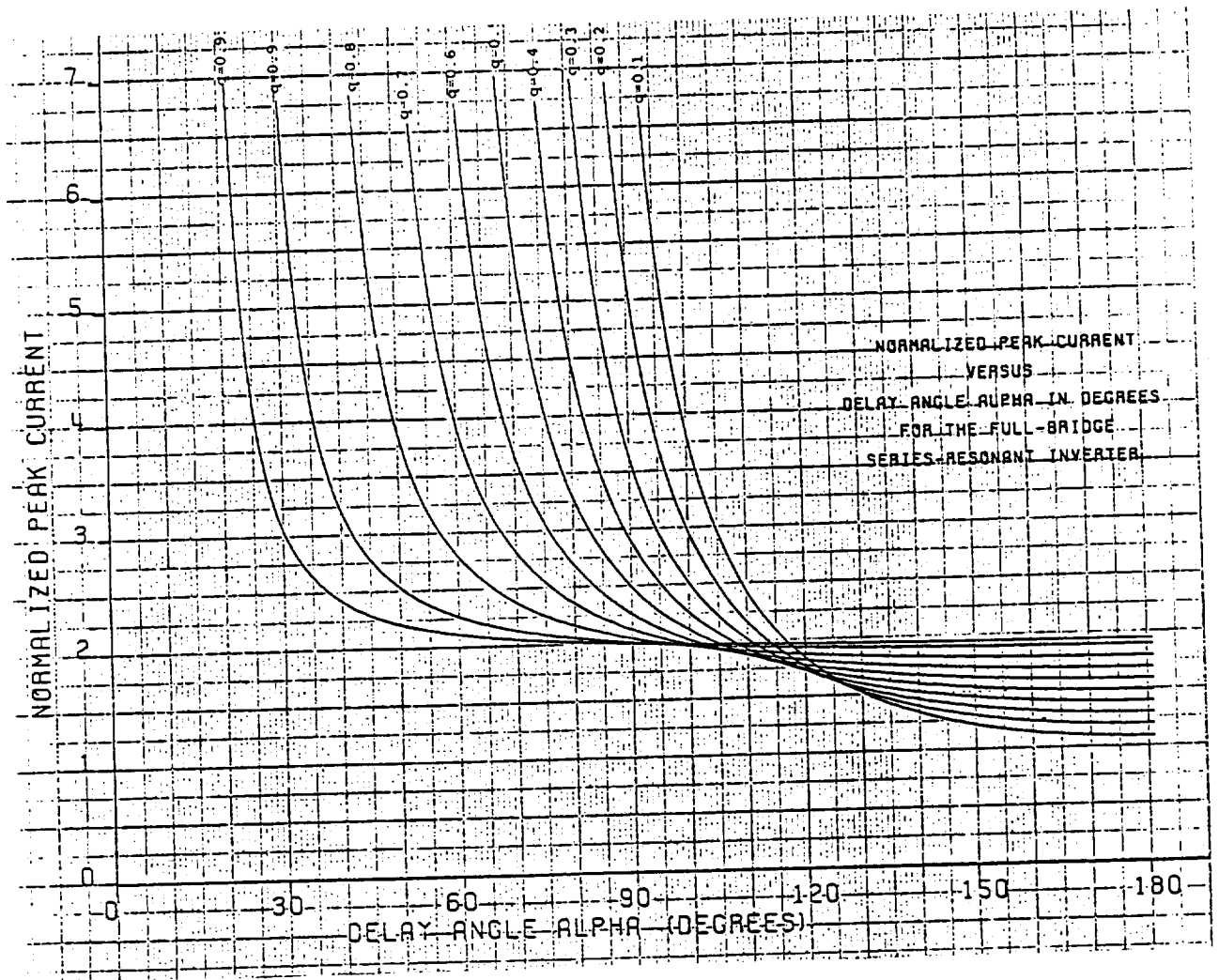


Fig II-9. I_{PN} vs α

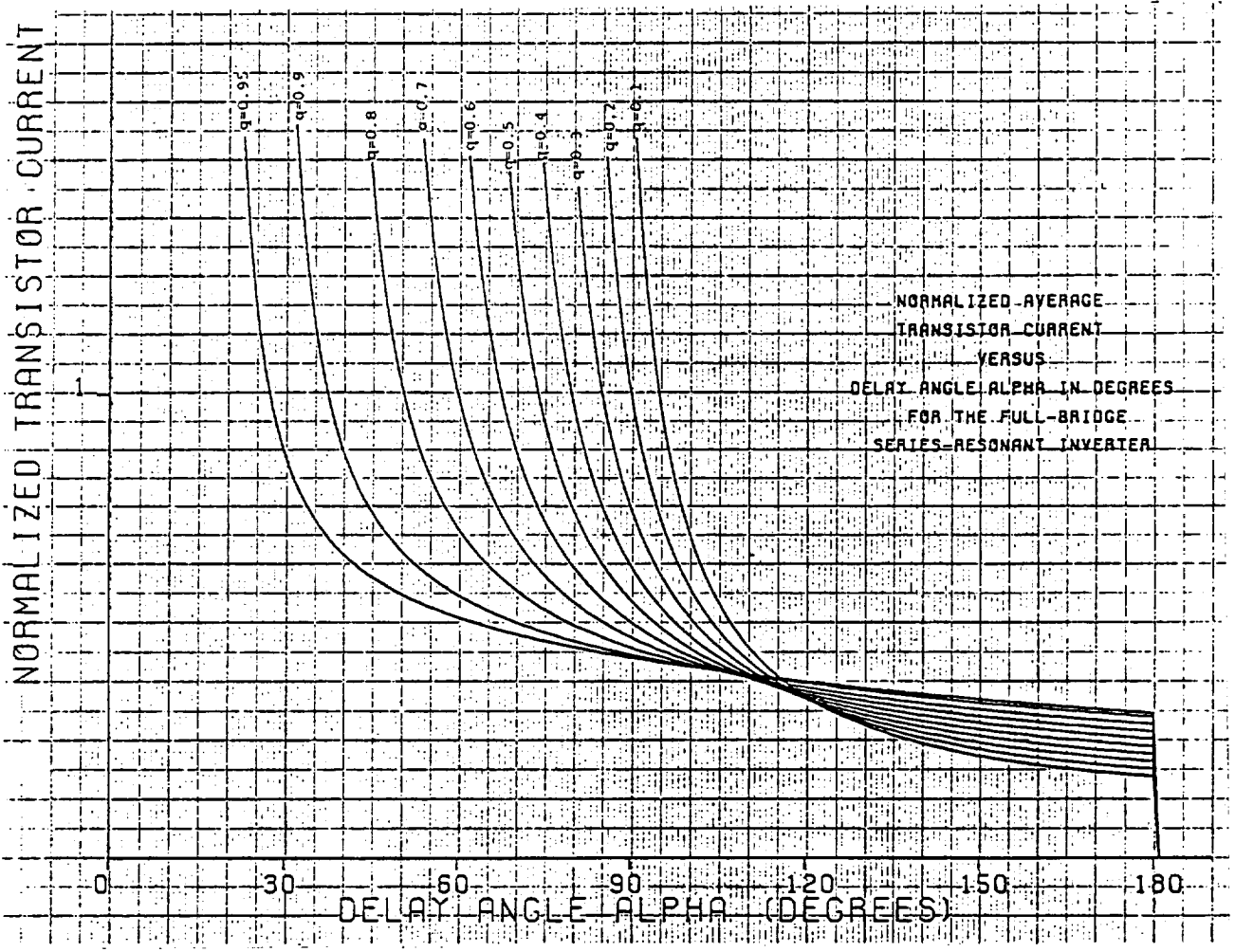


Fig II-10. I_{QN} vs α

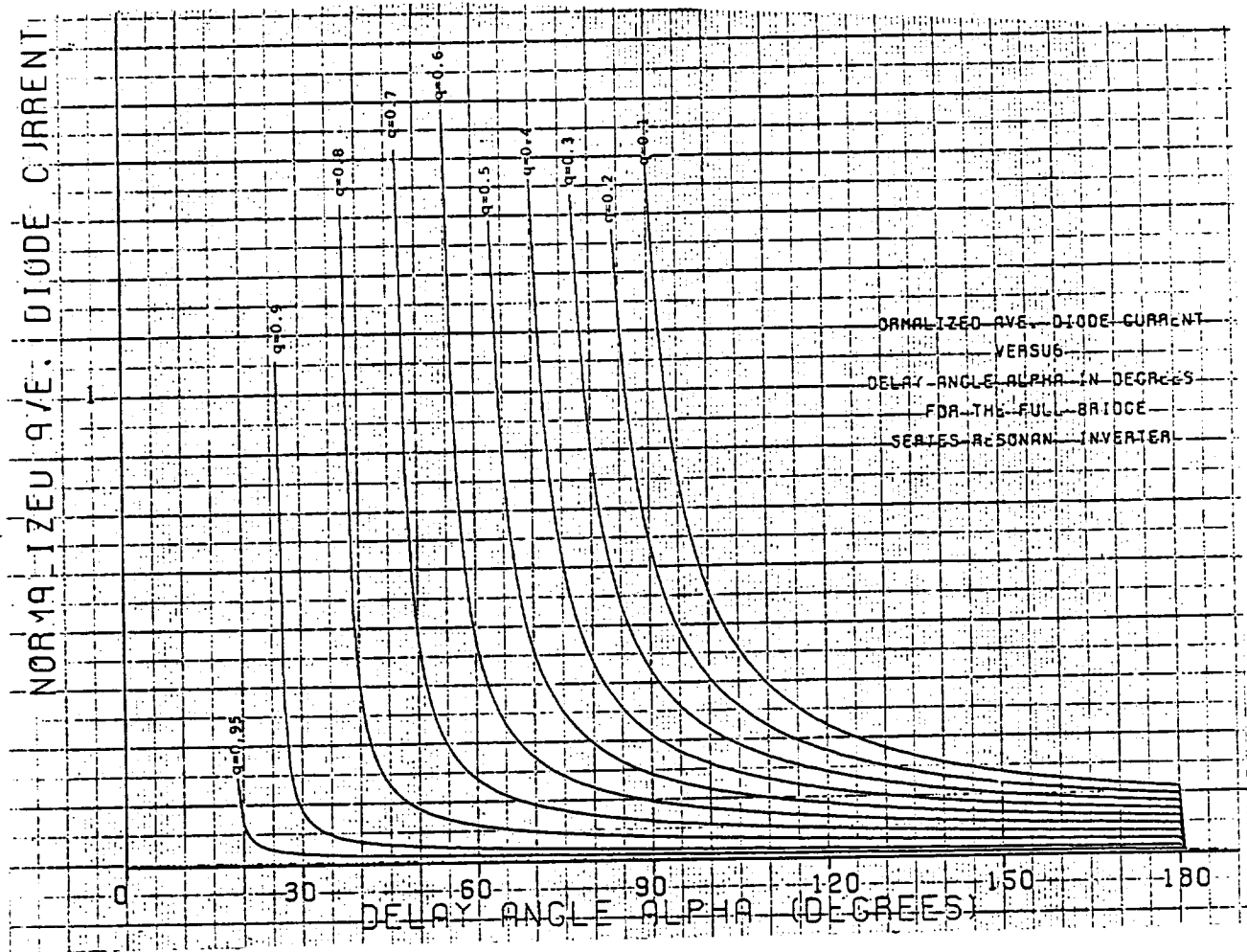


Fig II-11. I_{DN} vs α

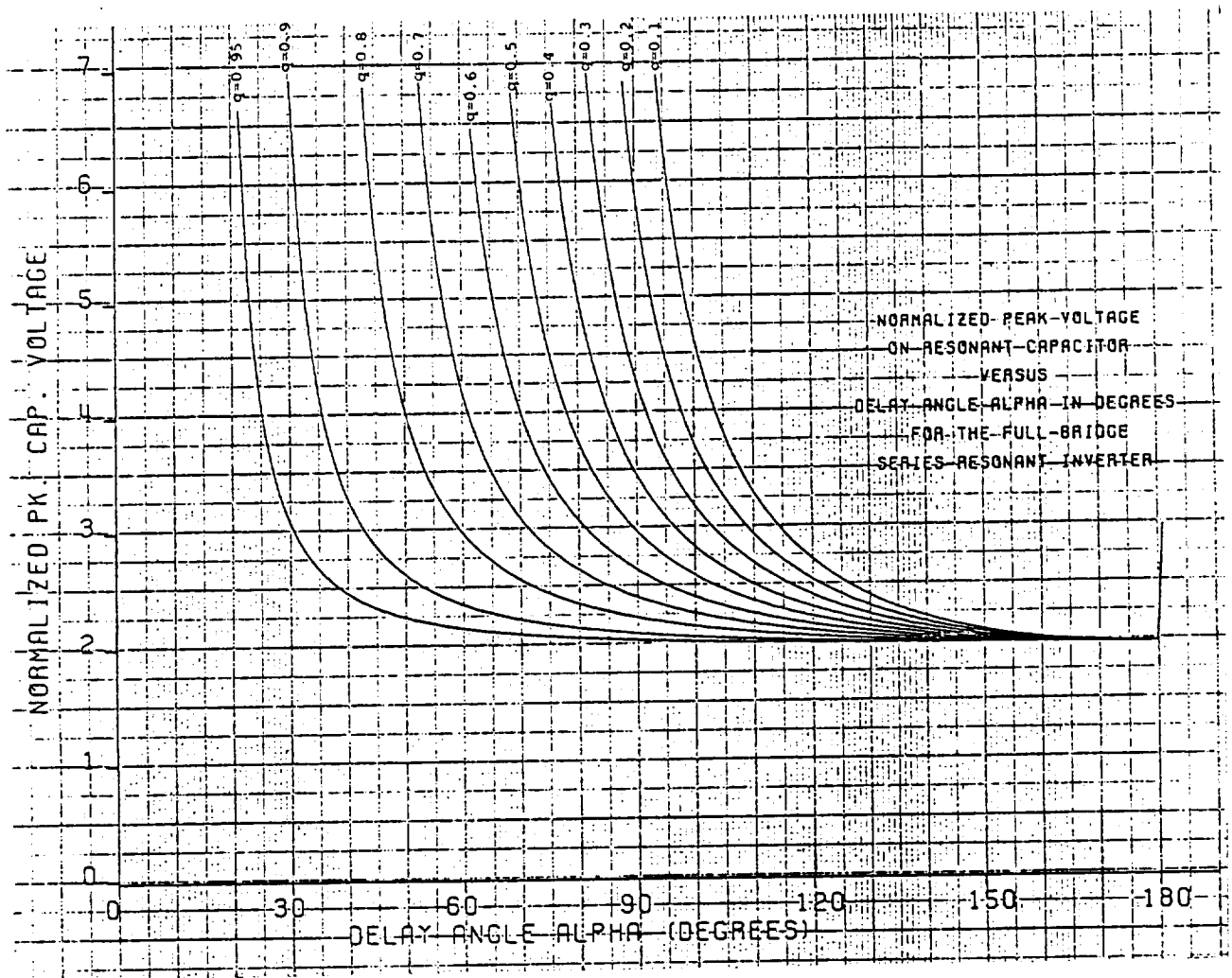


Fig II-12. V_{PN} vs α

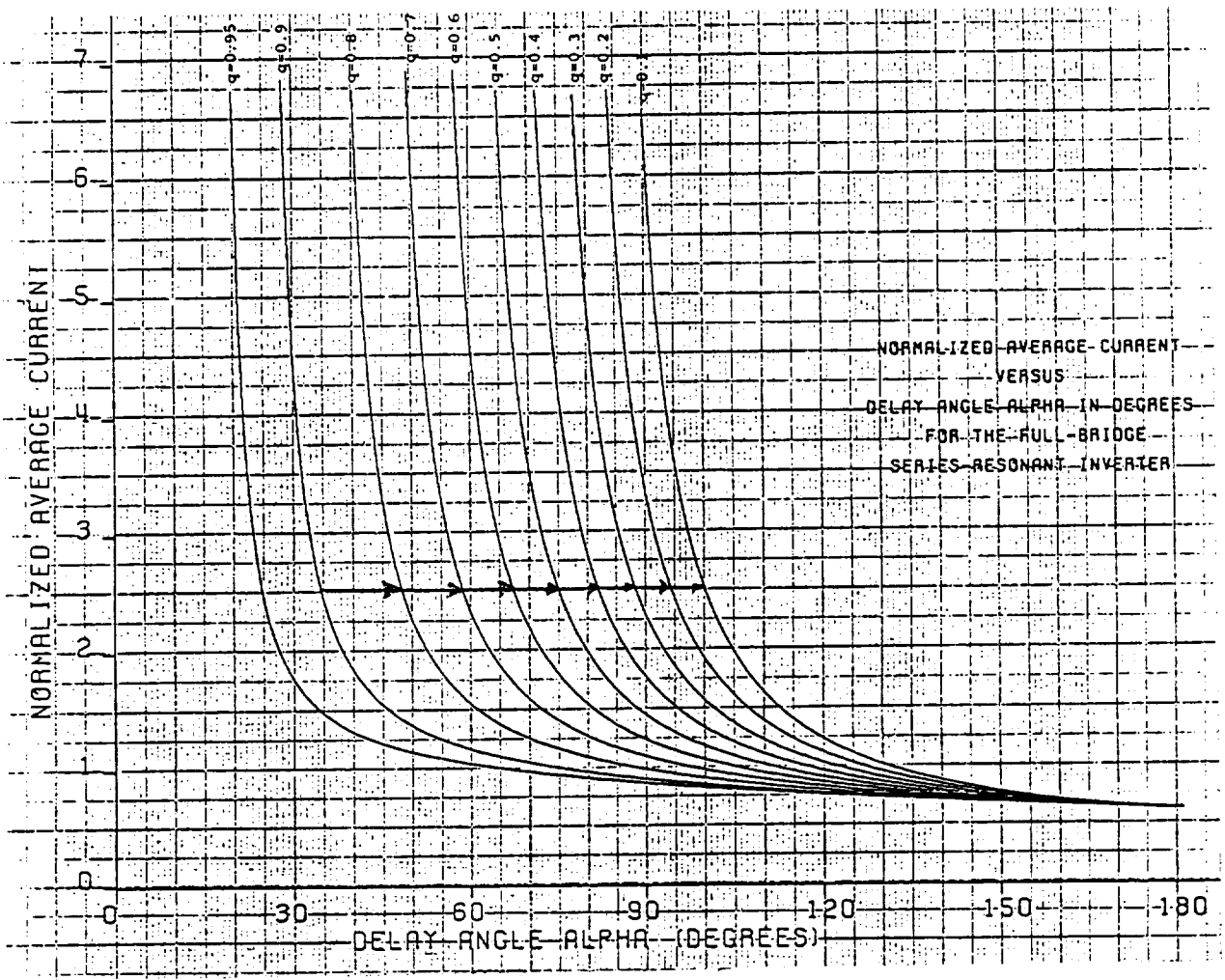


Fig II-13. I_{AN} vs α locus as q decreases.

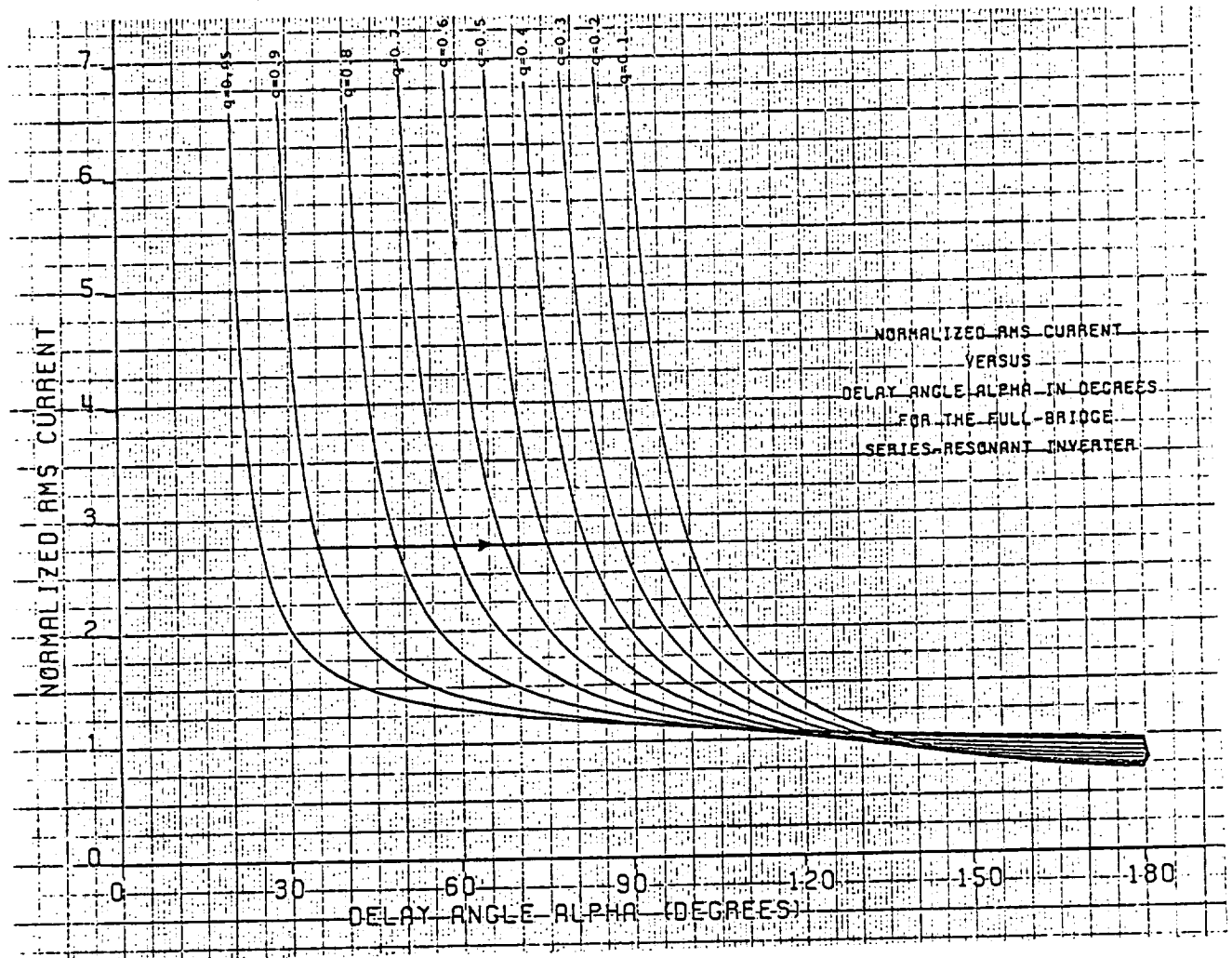


FIG II-14. I_{RN} vs α locus as q decreases.

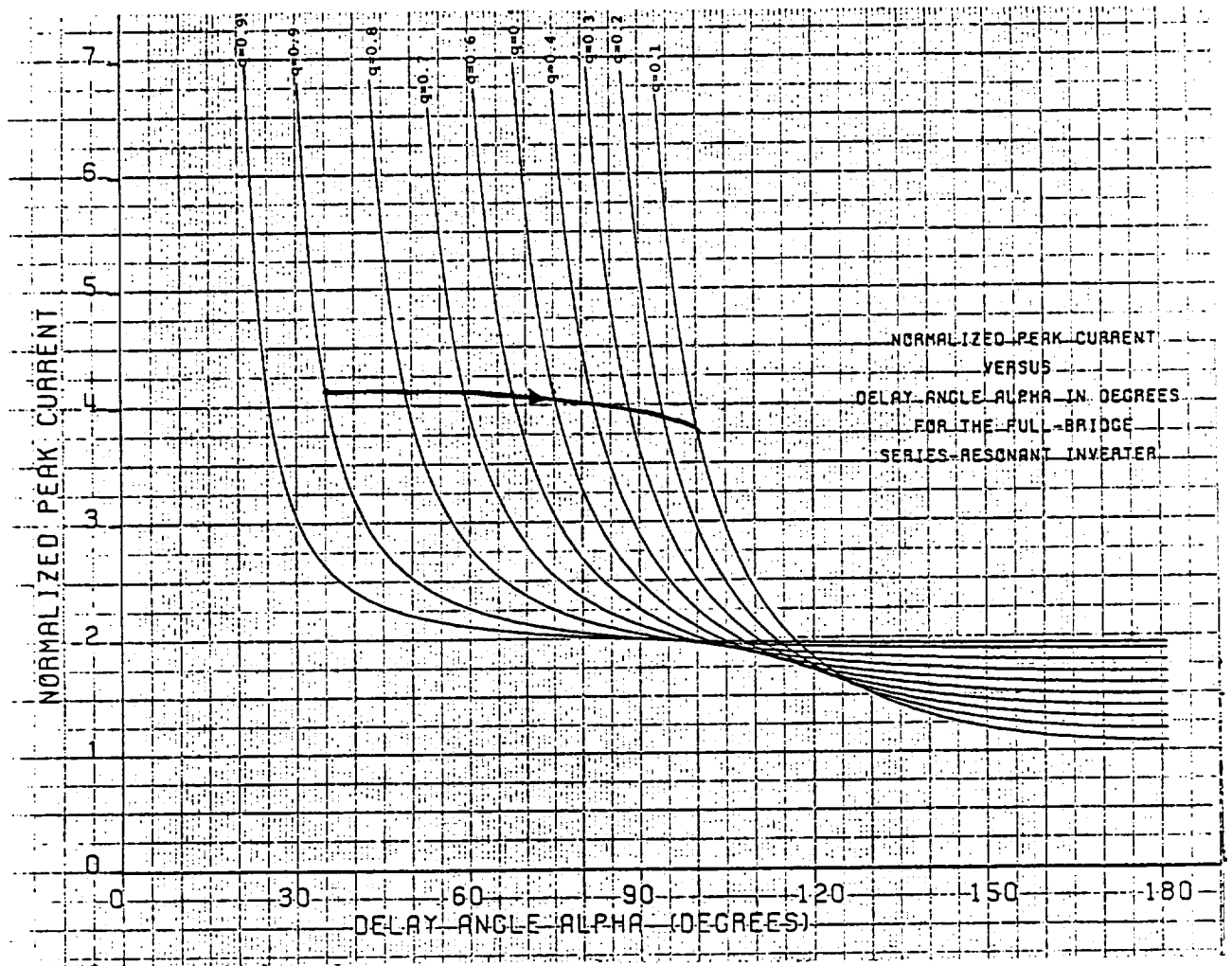


Fig II-15. I_{PN} vs α locus as q decreases.

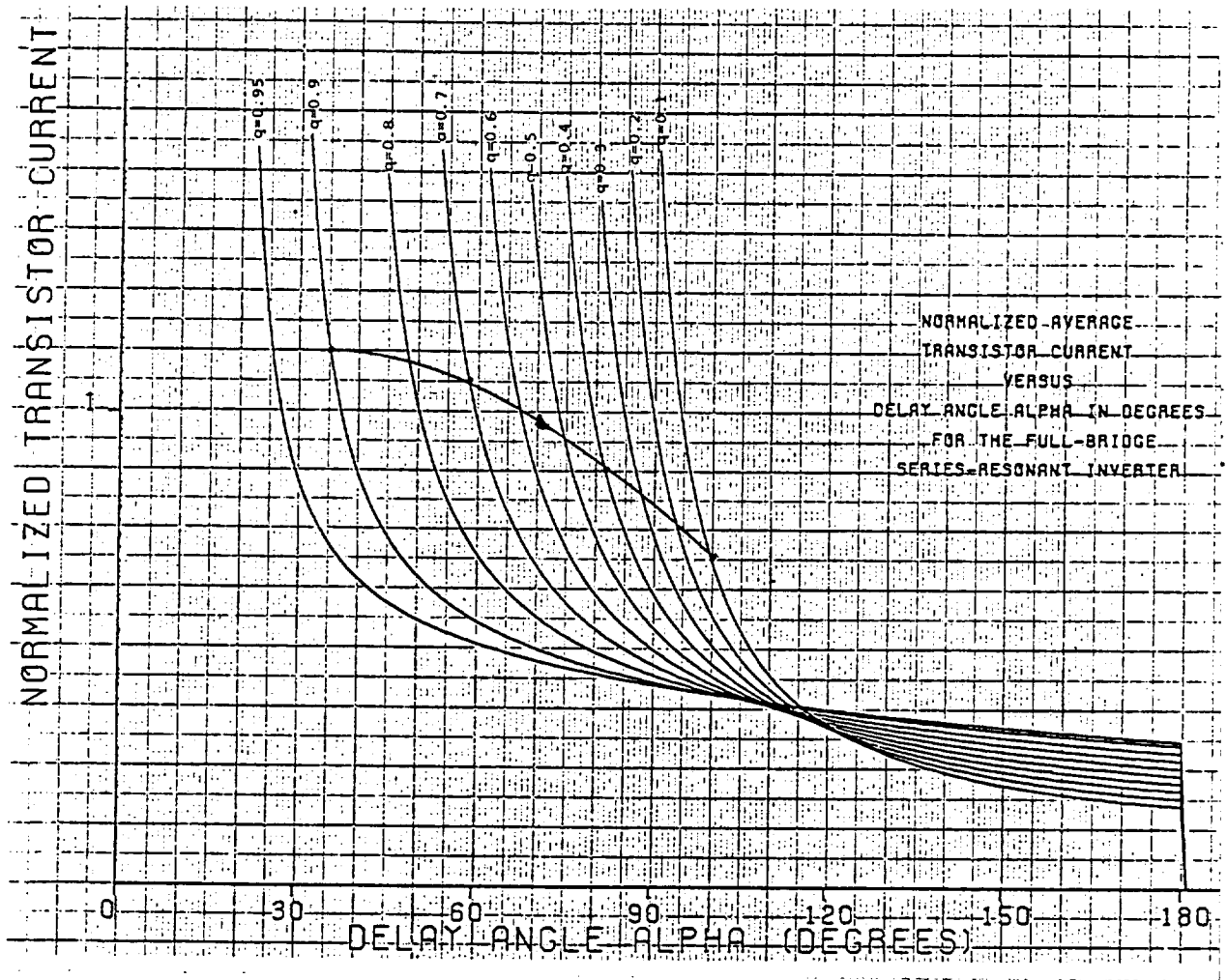


Fig II-16. I_{QN} vs α locus as q decreases.

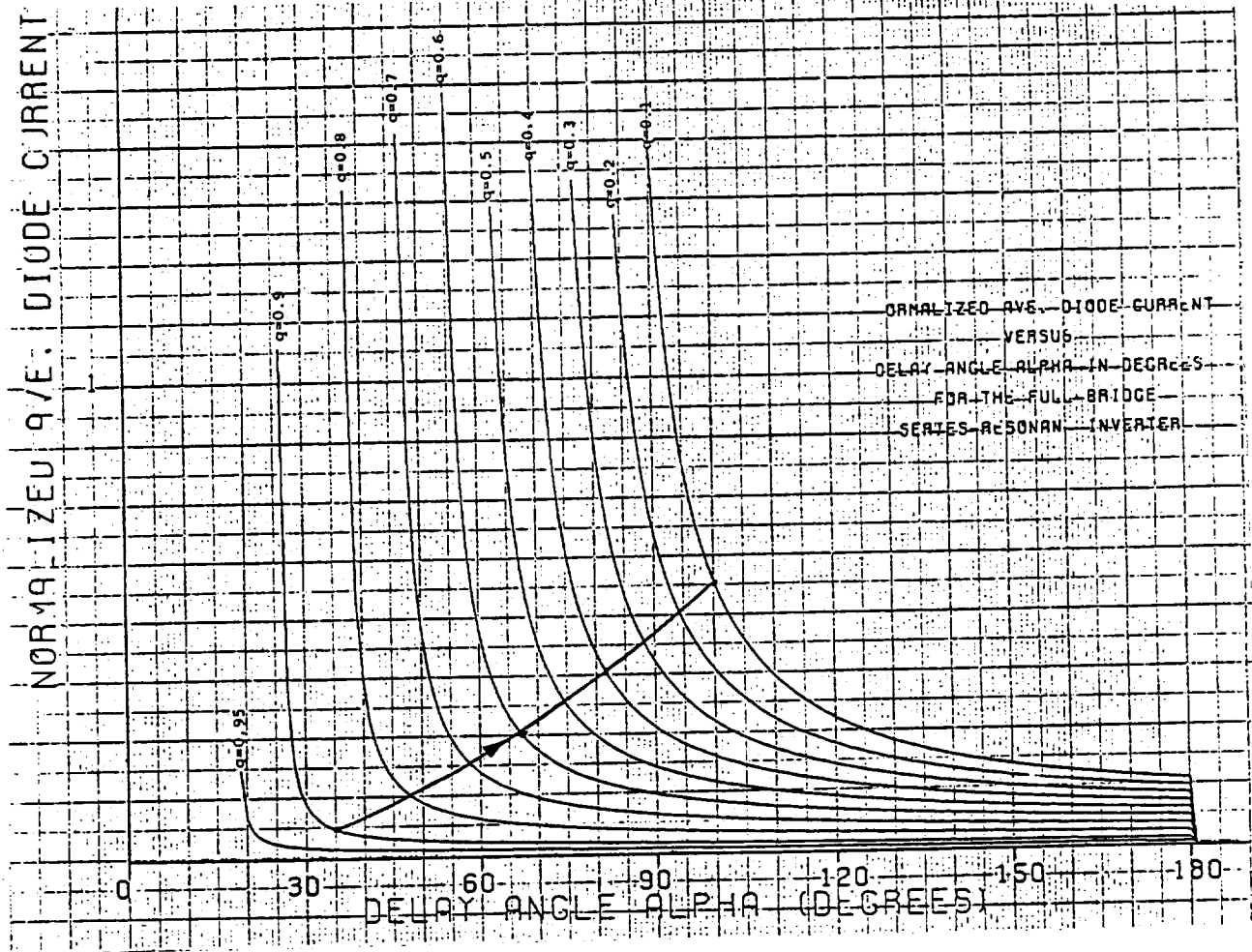


Fig II-17. I_{DN} vs α locus as q decreases.

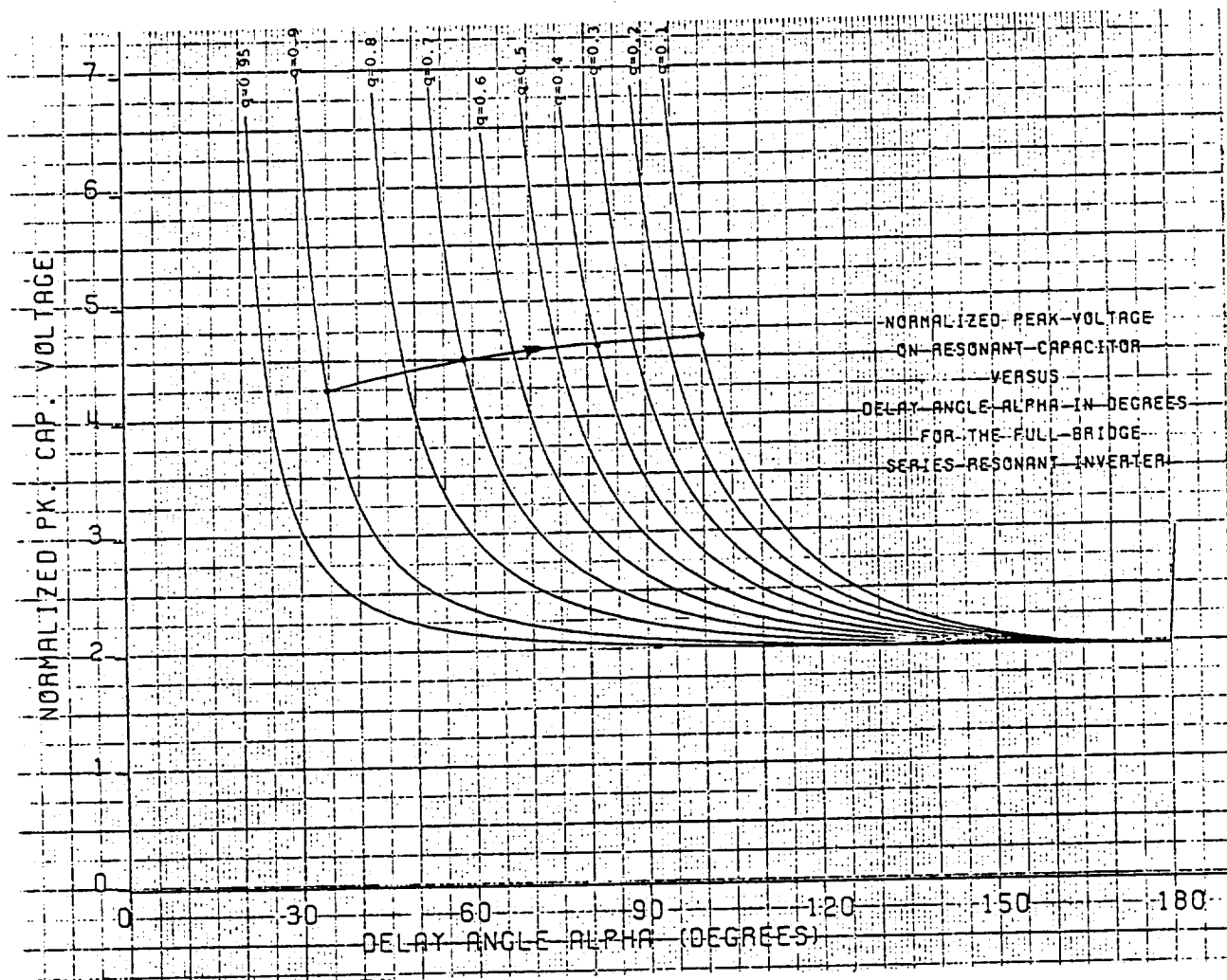


Fig II-18. V_{PN} vs α locus as q decreases.

III. POWER CIRCUIT PERFORMANCE AND EXPERIMENTAL DATA

A. Power Circuit Description

The power circuit diagram is reproduced in Fig. III-1 for convenience. Each switch in the full-bridge series-resonant converter comprises 3 paralleled MCTs (Harris developmental number MCTA60P60) and 1 anti-parallel diode (Harris developmental number RURU15060). The MCTs in one switching pole of the inverter were later changed to the Harris commercial part number MCTA75P60, considered to be a close equivalent of the developmental part. Because peak currents in steady state operation approached 250 A, with switched currents of nearly 150 A under some conditions, a low-inductance layout was used for the MCTs and the dc-side bypass capacitors. These values proved to be significantly higher than those from the initial design calculations because a lower value of α was eventually used. The mechanical layout of the MCTs and diodes is shown in Fig. III-2.

The purpose of the low-inductance assembly shown in Fig. III-2 is two-fold: One purpose is the control of the layout inductance, the other is the facilitation of removal and replacement of individual TO-218 packages without damage to the other devices. The assembly is composed of a 15.2-by-20.3-by-0.48 cm (6-by-8-by-3/16-inch) aluminum carrier plate, which does not carry current, together with 4 sub-assemblies bolted to it and insulated from it using 0.15-mm (6-mil) Wakefield type-175 Kapton thermally-conducting electrically-insulating material. Each sub-assembly is also built on 3/16-inch aluminum plate. One carries 6 MCTs and 2 diodes, forming two of the bridge switching legs, and also serving as the negative dc bus. This sub-assembly is marked "-dc" in Fig. II-2. Two other sub-assemblies carry 3 MCTs and 1 diode each, forming two more bridge switching legs and the two ac output terminals of the bridge. These sub-assemblies are marked "ac 1" and "ac 2" in the figure. All MCTs and diodes are mounted directly to their

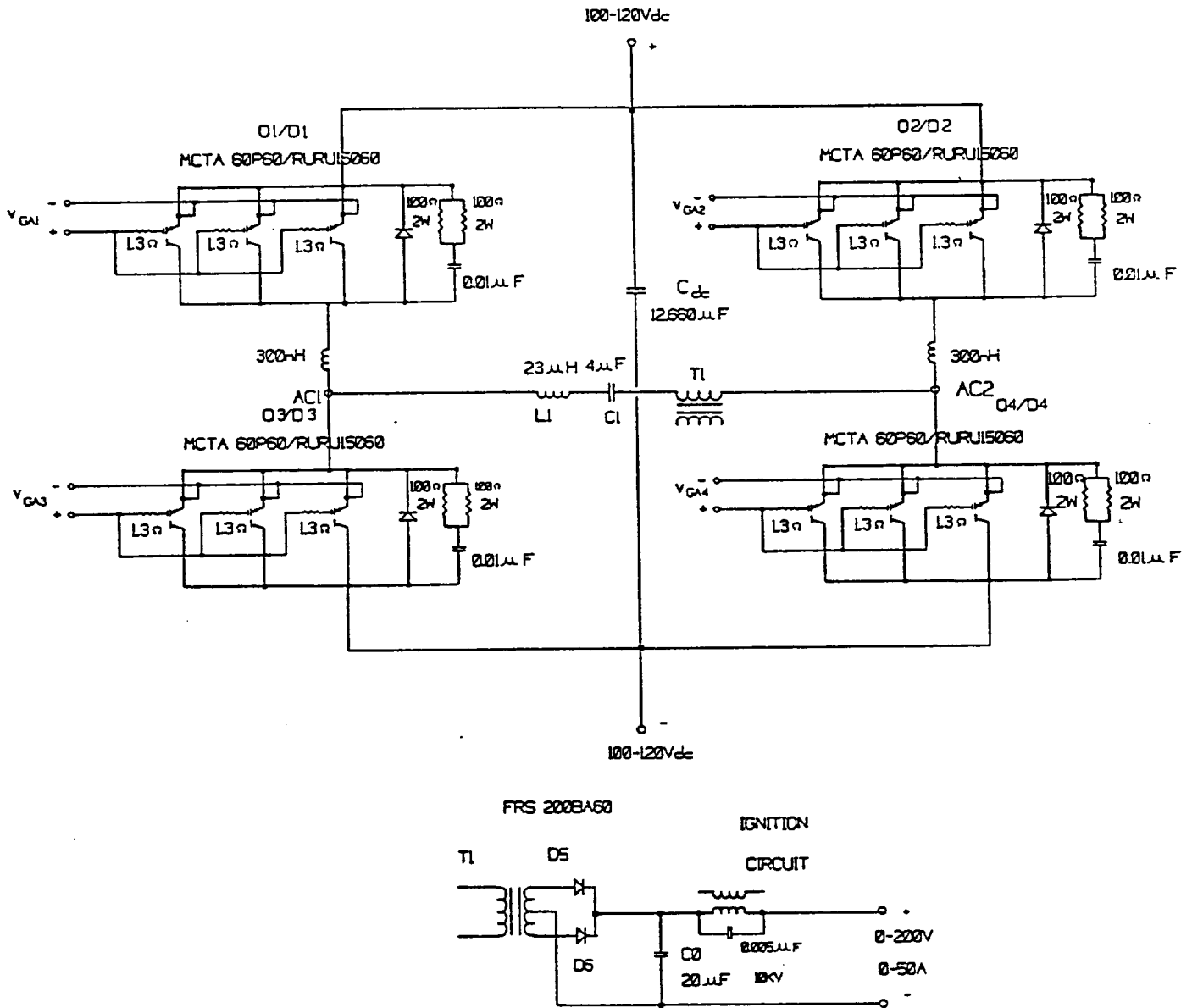


Fig. III-1 Power circuit of 10-kW 100-120 V arcjet power converter.

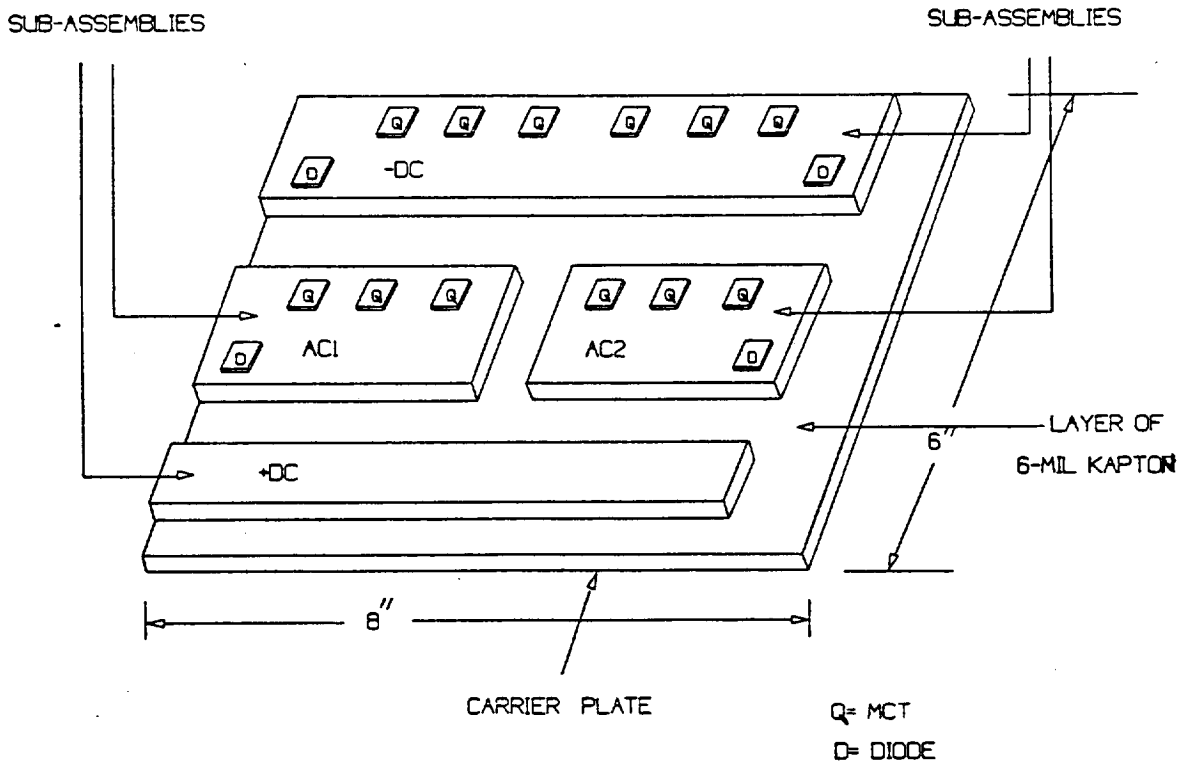


Fig. III-2 Mechanical layout for the switching devices of the 10-kW arcjet power converter.

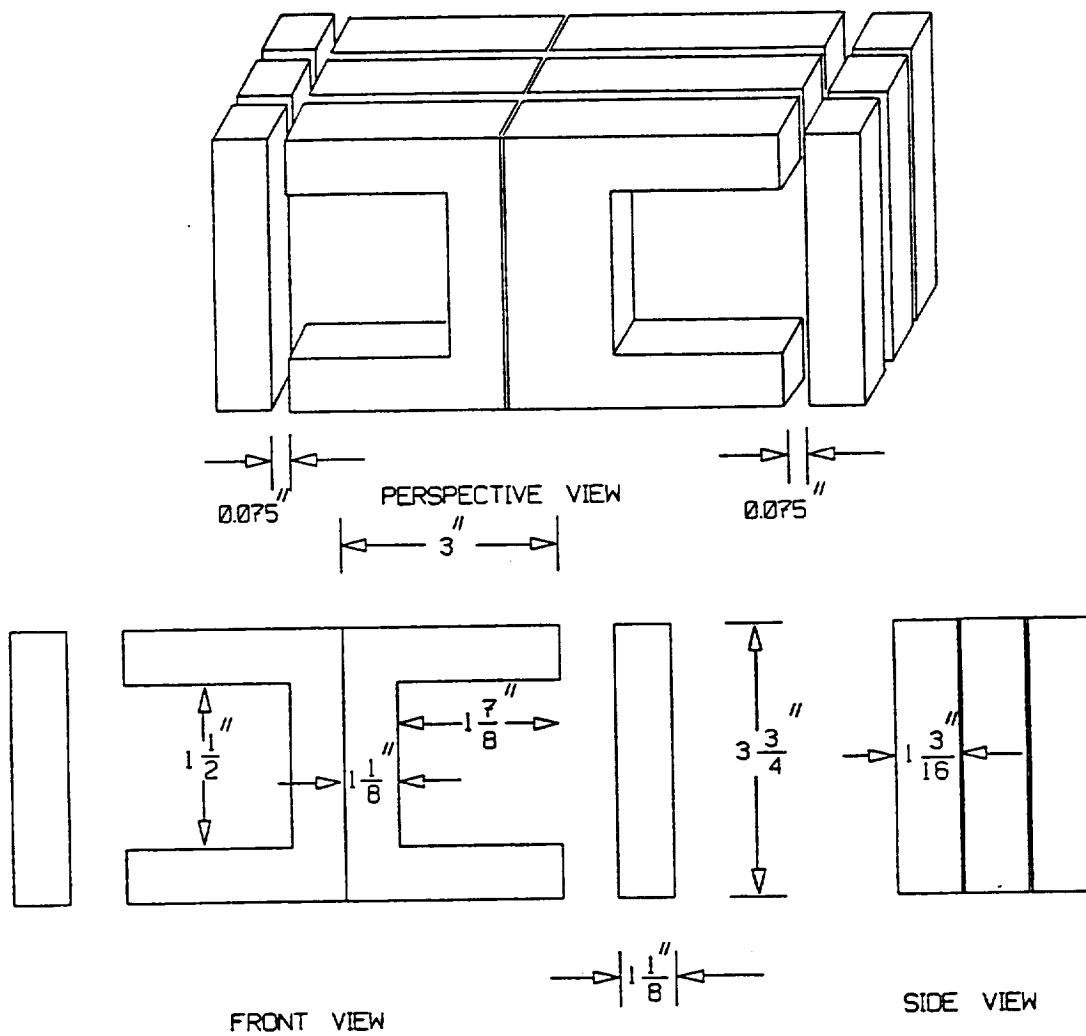


Fig. III-3 Core arrangement used for the 10-kW series-resonant inductor.

respective aluminum plates without any insulators. Heat flow from the switching devices is to their sub-assembly base plates, then through the Kapton insulating material to the aluminum carrier plate, and then to the cold plate to which the carrier plate is bolted.

Several comments can be made about this arrangement. One is that its heat flow properties can be very good if the problem of maintaining uniform pressure across the entire area of the sandwich of aluminum plates and insulators is properly solved. Space permitting, the sub-assembly base plates could be enlarged to spread the heat over a greater area before it passes through the insulator, thus lowering the net thermal resistance of this mounting system. Although it was not done on this project, EMI control could also be improved in some situations by adding a second layer of insulation between the aluminum carrier plate and the cold plate to which it is bolted. Connection to the carrier plate would then allow the redirection of the capacitive currents (displacement currents) through the insulating material away from the grounded cold plate.

It can also be noted that the arrangement described does not produce the lowest possible layout inductance because the commutating currents flow essentially side-by-side, although they have broad conducting paths. An alternative arrangement in which the commutating currents flow in facing layers of the structure would lower its inductance still farther, but was considered unnecessary here. The fairly low dc voltage of 100-120 V with the 600-V ratings of the MCTs made the control of voltage overshoot much less critical. Individual removal and replacement of the switching devices was also more readily possible with this mounting arrangement.

Approximately 300 nH of commutating inductance, shown in Fig. III-1, was added to each switching pole. This controls the di/dt of the commutations involving turn-off of the diode, and turn-on of the incoming MCT. Turn-off of the

MCTs is essentially lossless because of the operation of the series resonant tank below resonance. The snubbers were the simple R-C networks shown in Fig. III-1, and produced negligible snubbing losses relative to the power levels processed.

The resonant inductor (L1 in Fig. III-1) was found to be a substantial component, both in terms of size and losses. Three different arrangements with a small number of turns were tried, each using an air-gapped ferrite core assembly. Each was still found to be lossy, with excessive temperature rise in the copper windings. (In each case the core losses were small; the ferrite did not become hot until heat was transferred to it from the windings.) The final version of the inductor core is shown in Fig. III-3. This assembly of 3C8 ferrite C-I cores was wound with 3 turns (in 3 layers) of copper strap, consisting of two paralleled pieces 3.2 cm wide and 0.89 mm thick (1.25 by 0.035 in). Skin depth at 15 kHz is 0.54 mm (0.021 in), so no benefit from additional copper is expected. The magnetic path is air gapped in two places at approximately 1.9 mm (0.075 in), for a total gap of 3.8 mm. The inductance is 23 μ H at 250 A peak, for a stored energy of 0.72 J.

B. Steady-State Performance

The steady-state performance data for the converter is summarized in Table III-1, which lists the input-output conditions for four steady state operating points. These four test conditions are numbered in the table for later reference. Measured efficiencies ranged from 93.7% at partial load to 91.6% at full load of 201 V and 51.4 A output (10.3 kW).

Table III-1

Steady-State Performance Data for the 10-kW Arcjet Converter

	Input Voltage V_s	Input Current I_s	Input Power P_s	Output Voltage V_o	Output Current I_o	Output Power P_o	Power Effic.	Power Loss
1	120 V	58.0 A	6960 W	182.6 V	35.7 A	6519 W	93.7%	441 W
2	120 V	70.8 A	8496 W	153.1 V	49.5 A	7579 W	89.2%	918 W
3	120 V	78.0 A	9360 W	183.0 V	47.0 A	8592 W	91.8%	768 W
4	120 V	94.0 A	11280 W	201 V	51.4 A	10330 W	91.6%	949 W

Losses in the switching devices under the four conditions of Table III-1 were also measured. A Tektronix 11401 digital storage oscilloscope was used to sample the switch voltage and current waveforms for switch leg Q4/D4. These waveforms were event-averaged to reduce their noise levels, and then multiplied to form an instantaneous power waveform. This waveform was numerically integrated to determine the energy loss per switching period. The total Q1-Q4 and D1-D4 conduction and switching losses of the converter were then estimated by multiplying this result by 4. The data are summarized in Table III-2: The entries in this table correspond by row to those in Table III-1. Figs. III-4 through III-7 are also referenced in this table, and illustrate the switch loss-measurement data.

Table III-2

Measured Switching Device Losses, Based on the Q4/D4 Leg

	Switching Period	Switching Frequency	Energy	Power (1 Leg)	Power (4 Legs)	Total Converter Loss	See Figure
1	72.0 μ S	13.89 kHz	6.26 mJ	87.0 W	348 W	441 W	III-4
2	70.1 μ S	14.27 kHz	7.99 mJ	114 W	456 W	918 W	III-5
3	69.9 μ S	14.37 kHz	7.45 mJ	107 W	428 W	768 W	III-6
4	67.7 μ S	14.78 kHz	6.88 mJ	102 W	407 W	949 W	III-7

Waveforms showing the details of the switching in the Q4/D4 leg are in Figs. III-8 and III-9. Fig. III-8 shows the turn-on transition. The upper window in this figure shows the MCT anode-cathode voltage (v_{AK} , 100 V/div), anode current (i_A , 50 A/div) and gate-anode voltage (v_{GA} , 20 V/div). The operating conditions were an input voltage of 120 V, and output voltage of 137 V at 49.7 A, so the switched currents were close to those of full-power operation. (The turn-on current actually exceeds that of full-power by about 25 A.) The lower window of Fig. III-8 shows the turn-on waveforms for this switch at 500 nS/div. It can be noted that turn-on of the MCT occurs with a *negative* gate-anode voltage, thus requiring gate drive polarity inverted from the usual arrangement. The manufacturer recommends a positive gate voltage to ensure turn-off of the MCTs. This raises questions of reliability in that the system must be designed to supply turn-off bias to the MCTs prior to the application of anode voltage. The turn-on transition in Fig. III-8 lasts about 500 nS and is lossy. A shelf of about 160 nS may be observed on the falling edge of the anode voltage waveform. Increased commutating inductance could be used to reduce this switching loss, at the expense of increased snubbing loss, but this was not done. Fig. III-7 shows that

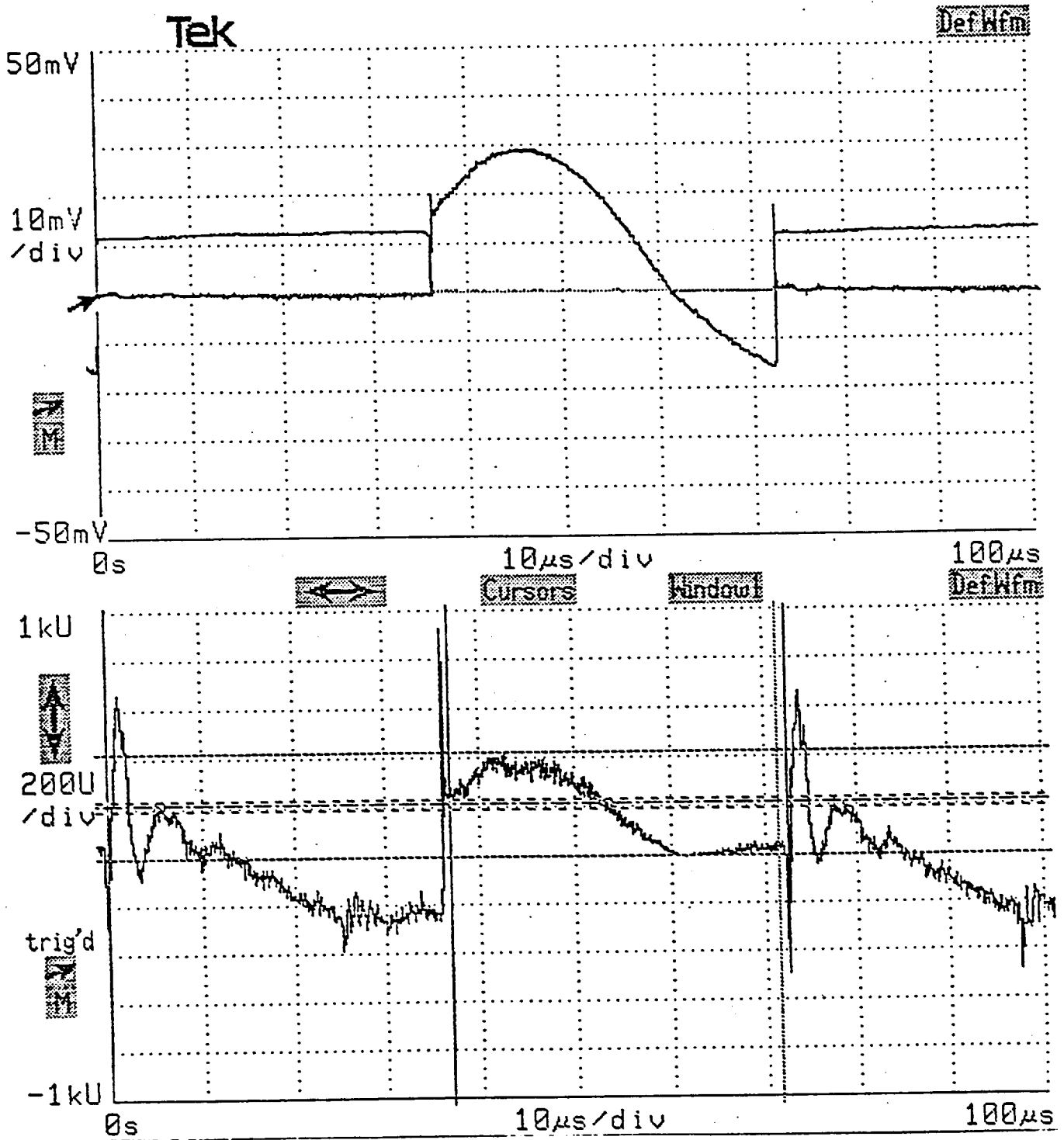


Fig. III-4 Steady-state operation, case 1. Switch loss measurement (refer to Table III-2).

Upper window: Switch current (50 A/div)

Switch voltage (100 V/div)

Lower window: Switch instantaneous power (200 W/div)

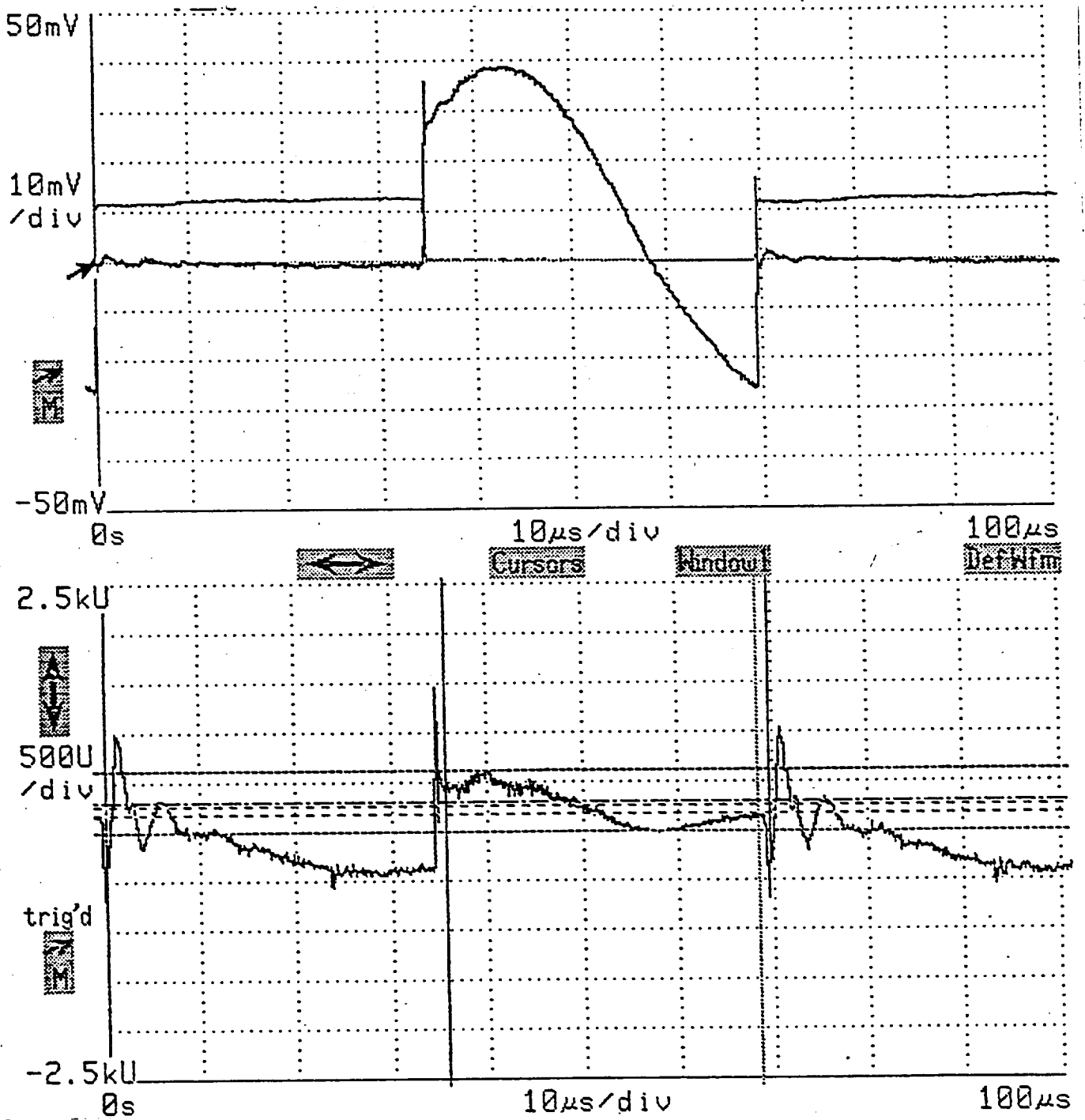


Fig. III-5 Steady-state operation, case 2. Switch loss measurement (refer to Table III-2).

Upper window: Switch current (50 A/div)

Switch voltage (100 V/div)

Lower window: Switch instantaneous power (500 W/div)

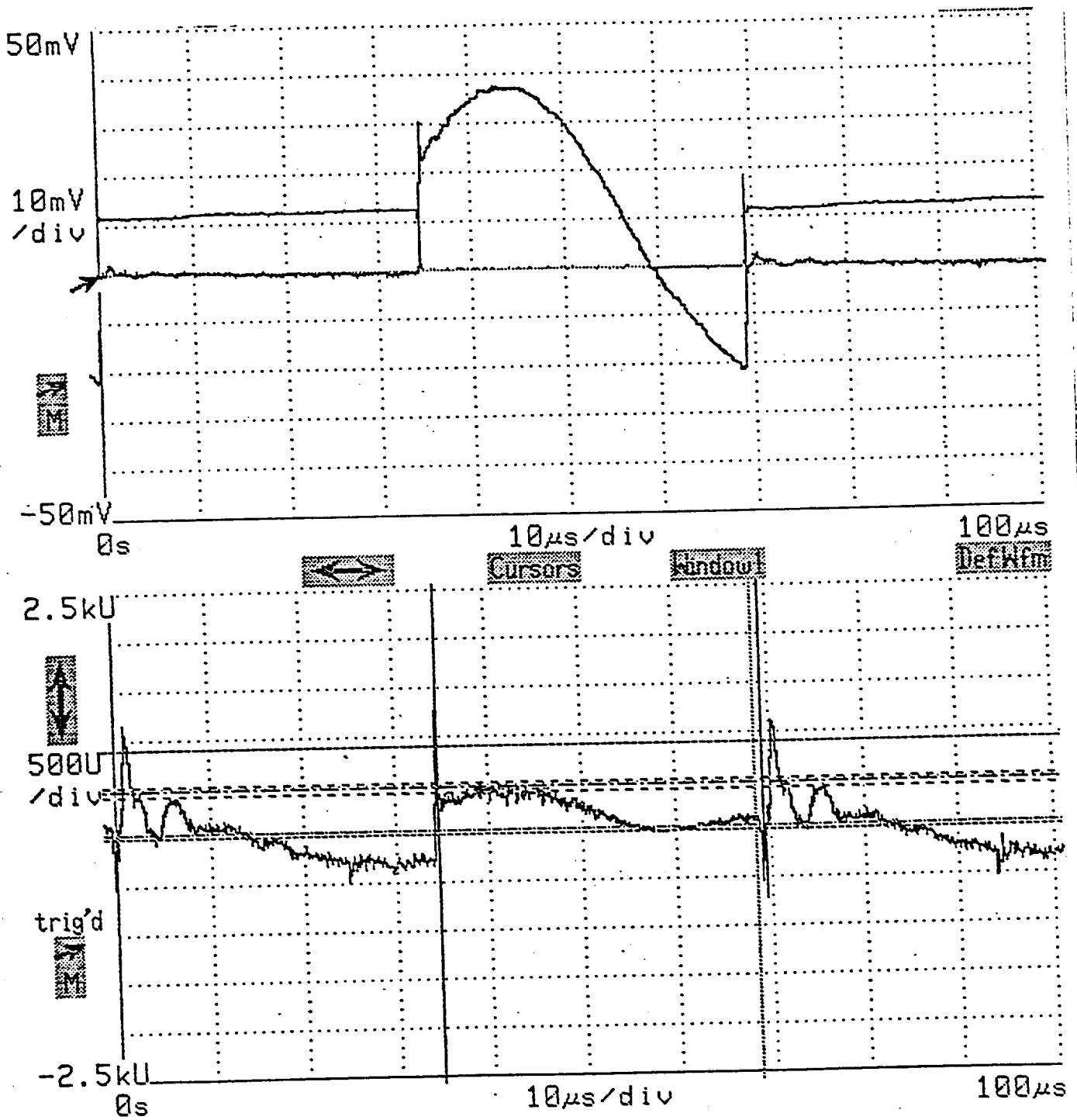


Fig. III-6 Steady-state operation, case 3. Switch loss measurement (refer to Table III-2).

Upper window: Switch current (50 A/div)

Switch voltage (100 V/div)

Lower window: Switch instantaneous power (500 W/div)

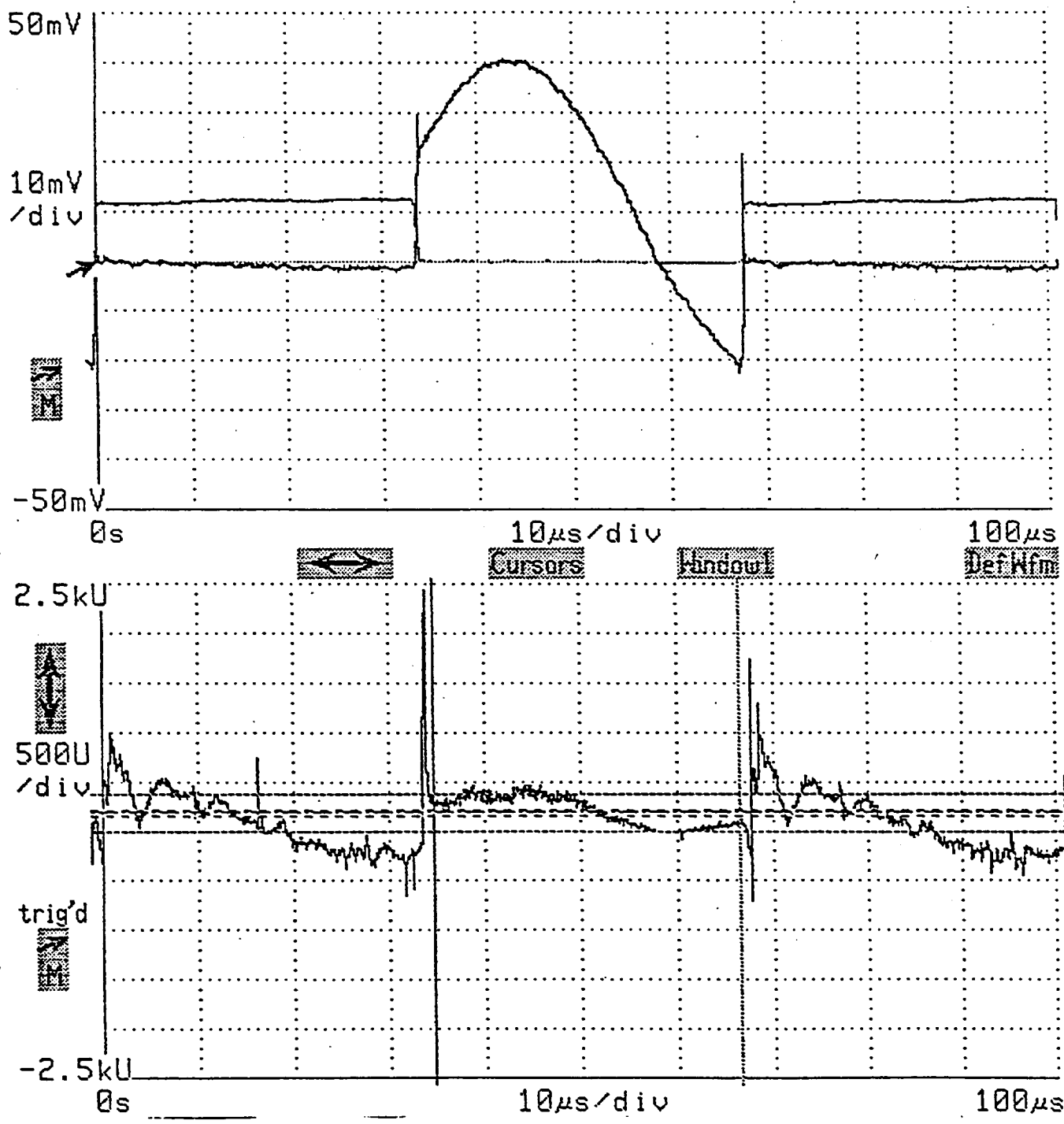


Fig. III-7 Steady-state operation, case 4. Switch loss measurement (refer to Table III-2).
 Upper window: Switch current (50 A/div)
 Switch voltage (100 V/div)
 Lower window: Switch instantaneous power (500 W/div)

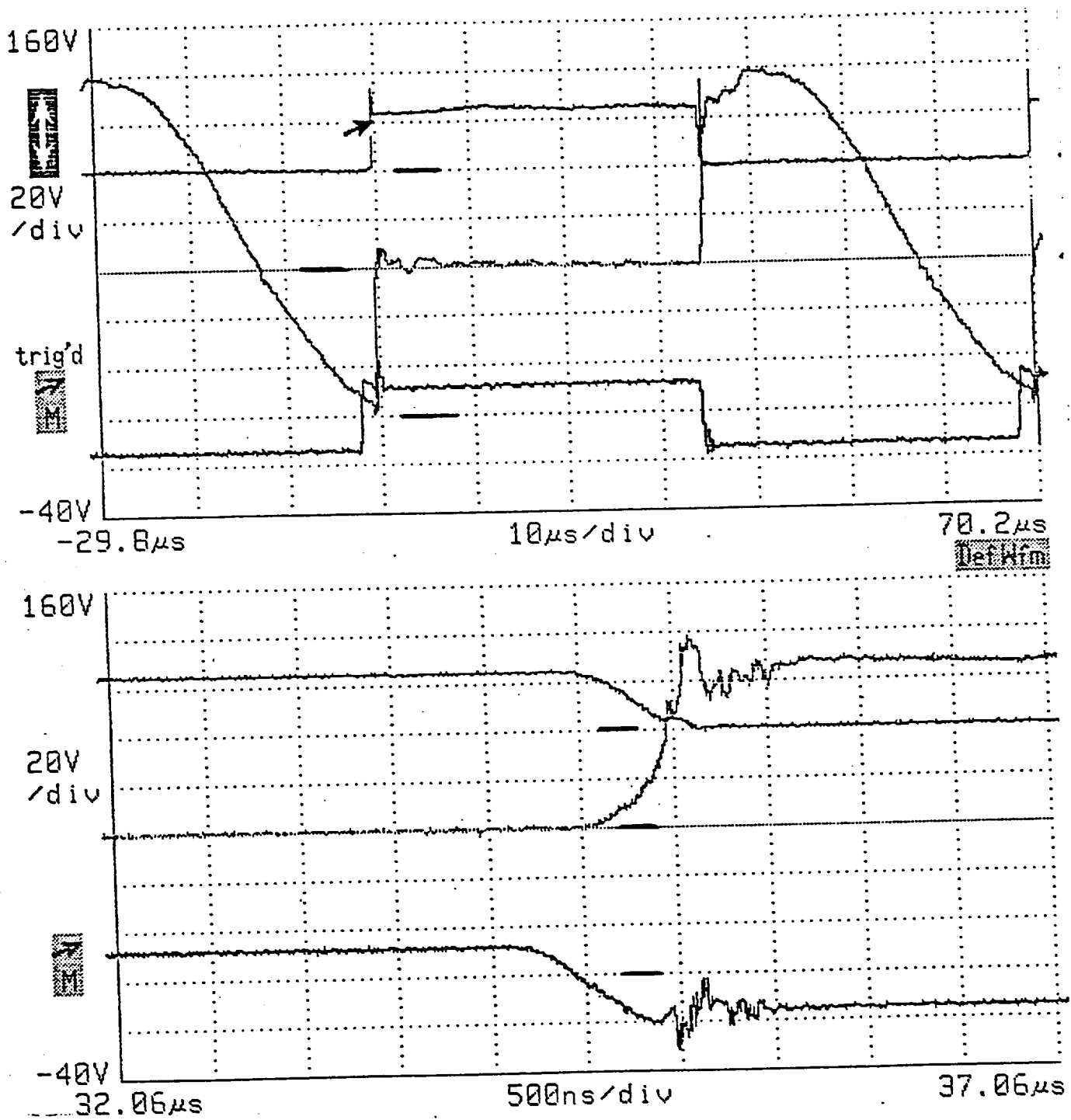


Fig. III-8 Switch turn-on loss, operation with 137 V/50 A output (6850 W).

Upper window: Switch voltage (100 V/div)
 Switch current (50 A/div)
 Gate-anode voltage (20 V/div)
 at 10 μS/div. Baselines indicated.

Lower window: Same as upper window, except timebase is 500 nS/div.

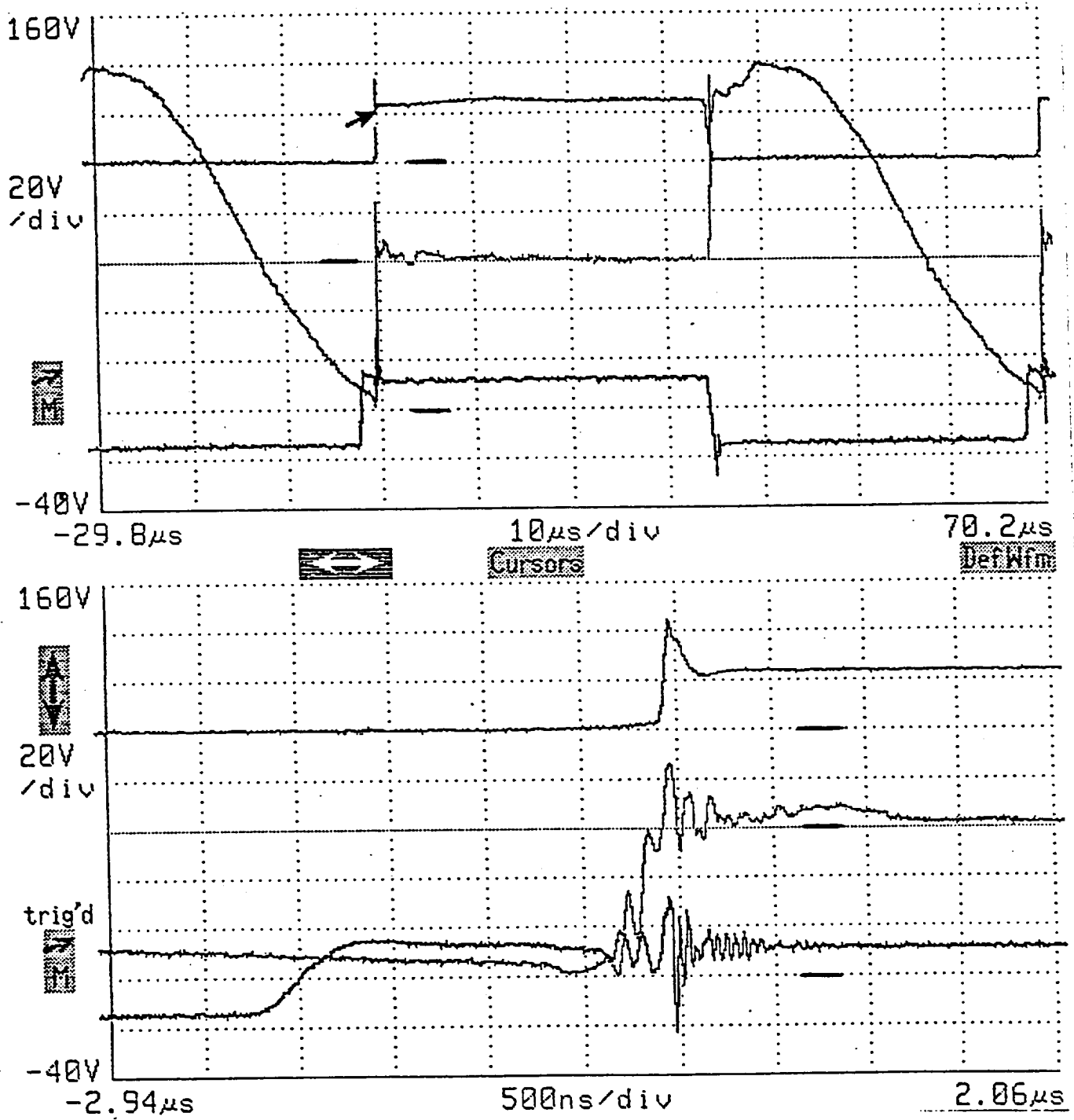


Fig. III-9 Switch turnoff loss, operation with 137 V/50 A output (6850 W).

Upper window: Switch voltage (100 V/div)

Switch current (50 A/div)

Gate-anode voltage (20 V/div)

at 10 μs/div. Baselines indicated.

Lower window: Same as upper window, except timebase is 500 ns/div.

although there is an impulse of loss at turn-on exceeding 2.5 kW, its approximate energy content is only 0.75 mJ, thus its contribution relative to the conduction loss is not great.

The turn-off transition is detailed in Fig. III-9 for the same operating conditions as Fig. III-8. The upper window of this figure also shows the MCT anode-cathode voltage (v_{AK} , 100 V/div), anode current (i_A , 50 A/div) and gate-anode voltage (v_{GA} , 20 V/div). The lower window shows the turn-off waveforms at 500 nS/div. This switching transition is lossless for the MCT due to the below-resonance operation of the series-resonant converter. It may be seen that the gate-anode voltage has made its transition to the off state well in advance of the current commutation, and also that turn-off losses for the anti-parallel diode are low. The diodes, Harris developmental device RURU15060 with a rated recovery time of 90 nS, did quite well in this regard compared to other 600 V/150 A diodes. Below-resonance operation was selected for use with the MCTs because of the lengthy current fall time (1.4 μ S) specified for this device.

C. Load Transient Tests

The transient response of the dc/dc converter was explored using stepped load changes. The converter was loaded with a resistive load bank, connected directly across the 20 μ F output capacitor (the 200 μ H inductor in the ignition circuit was not included). Fig III-10 shows the results of a step increase in the load resistance. The output current (center of Fig. III-10, 50 A/div) is virtually unaffected by a doubling of the load resistance. The output voltage (top of Fig. III-10, 100 V/div) nearly doubles. The transient in the resonant tank current can be seen at the bottom of the figure (200 A/div) to be very small.

Fig. III-11 shows the transient due to a step decrease in the load resistance. Here the load voltage (top of Fig. III-11, 100 V/div) halves following the transient. The load current (center, 50 A/div) shows a momentary overshoot of about 38 A

and then returns to its set point of 50 A. There is a transient overcurrent in the resonant tank current (bottom, 200 A/div), but it is of quite manageable size. Flux capacity for this transient should be allowed in the design of the resonant inductor, but it is probable that the flux density needed for a low-loss design will ensure this.

The effects of the 200 μ H output inductor in the ignition circuit were next explored. Fig. III-12 shows the transient produced by a load resistance step increase with the output inductor in place. This waveform is virtually the same as that of Fig. III-10, showing that the 200 μ H inductor produces a insignificant time constant, relative to the others associated with the resonant converter. Fig. III-13 shows the transient produced by a load resistance step decrease. Again, the result is virtually the same as that of Fig. III-11. This transient is also shown on a different time scale (5 mS/div) in Fig. III-14. Both the 20- μ F capacitor voltage (top, 100 V/div) and the load voltage (next down, 100 V/div) are shown in Fig. III-14. It can be seen that the inductor contributes negligible dynamics on this time scale, although it does serve to filter the load current ripple.

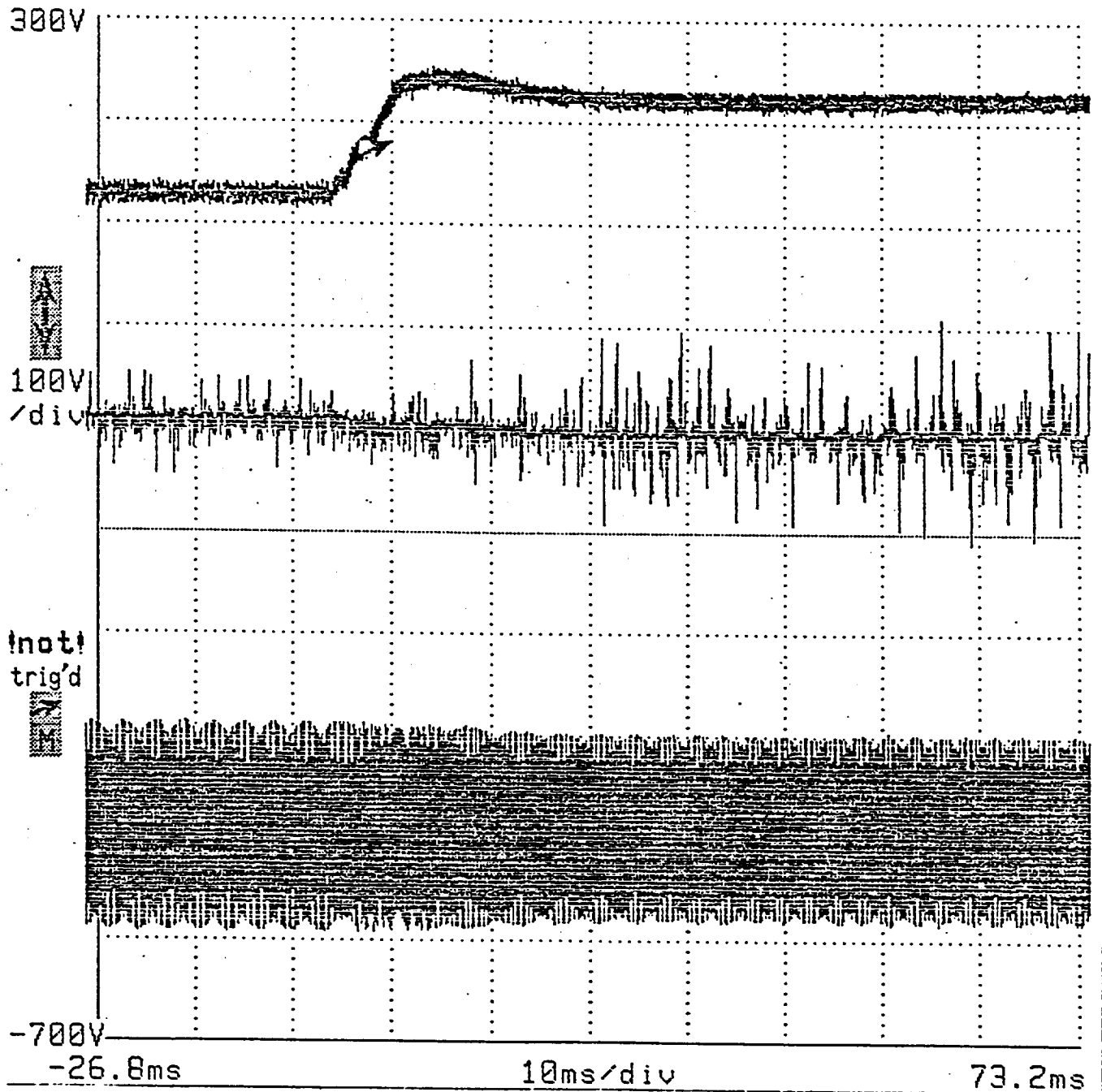


Fig. III-10 Load-resistance step-increase-transient with initial operation at 130 V, 50 A.
Ignition circuit not in place.

Upper: Load voltage (100 V/div).

Middle: Load current (50 A/div).

Lower: Resonant tank current (200 A/div).

Timebase: 10 mS/div.

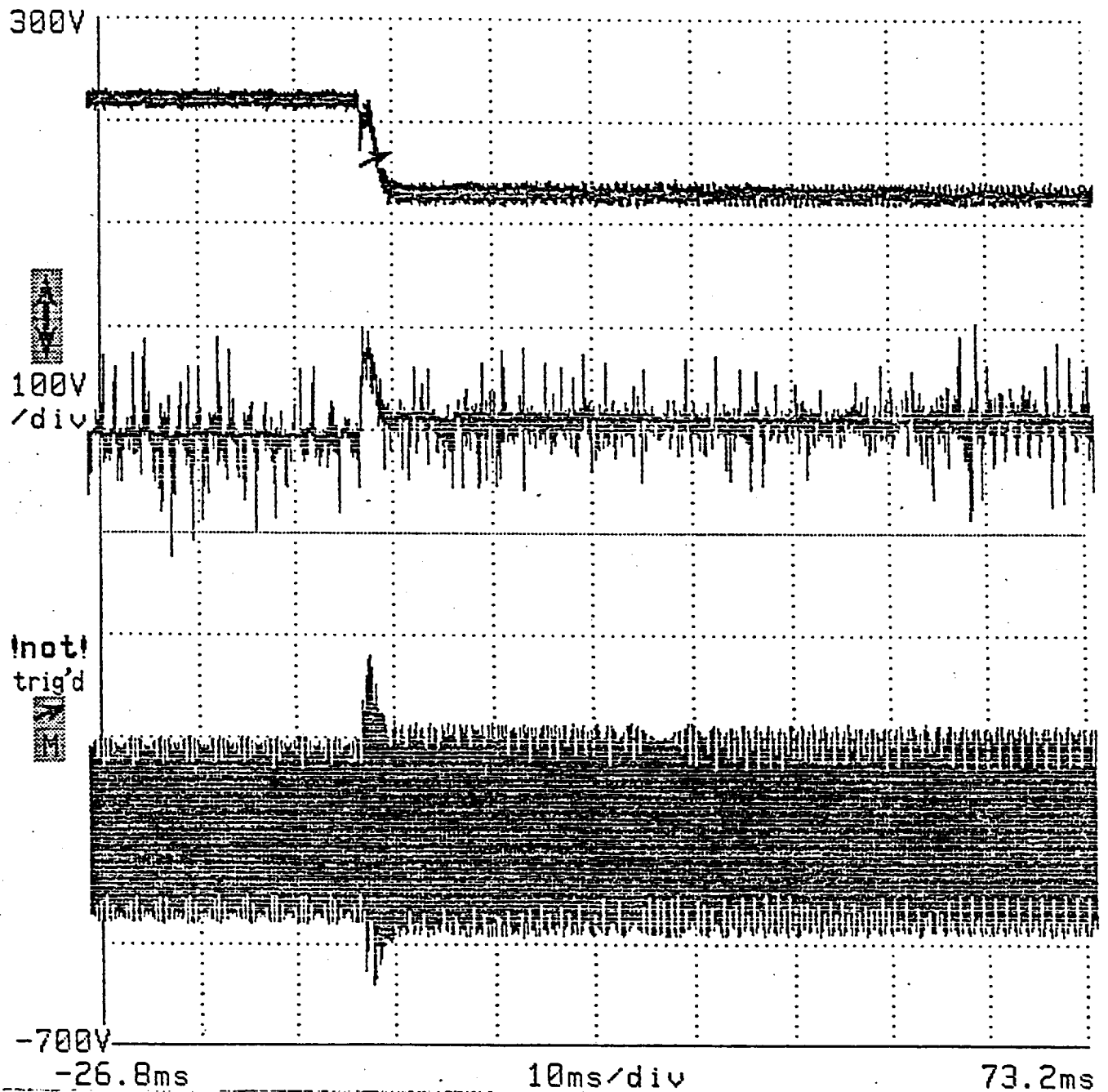


Fig. III-11 Load-resistance step-decrease-transient with initial operation at 220 V, 50 A.
Ignition circuit not in place.

Upper: Load voltage (100 V/div).

Middle: Load current (50 A/div).

Lower: Resonant tank current (200 A/div).

Timebase: 10 mS/div.

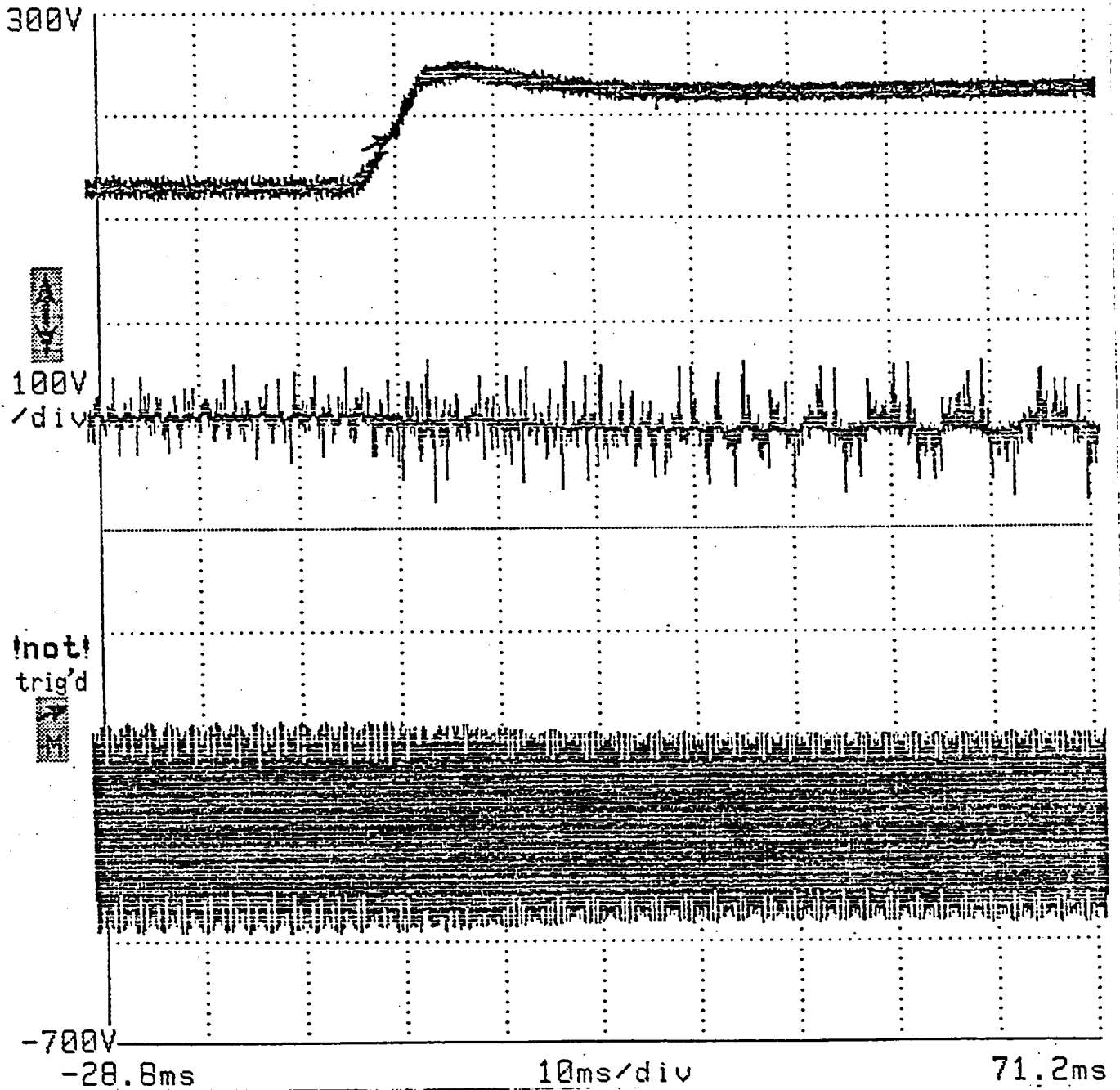


Fig. III-12 Load-resistance step-increase-transient with initial operation at 130 V, 50 A. Ignition circuit in place.

Upper: Load voltage (100 V/div).

Middle: Load current (50 A/div).

Lower: Resonant tank current (200 A/div).

Timebase: 10 mS/div.

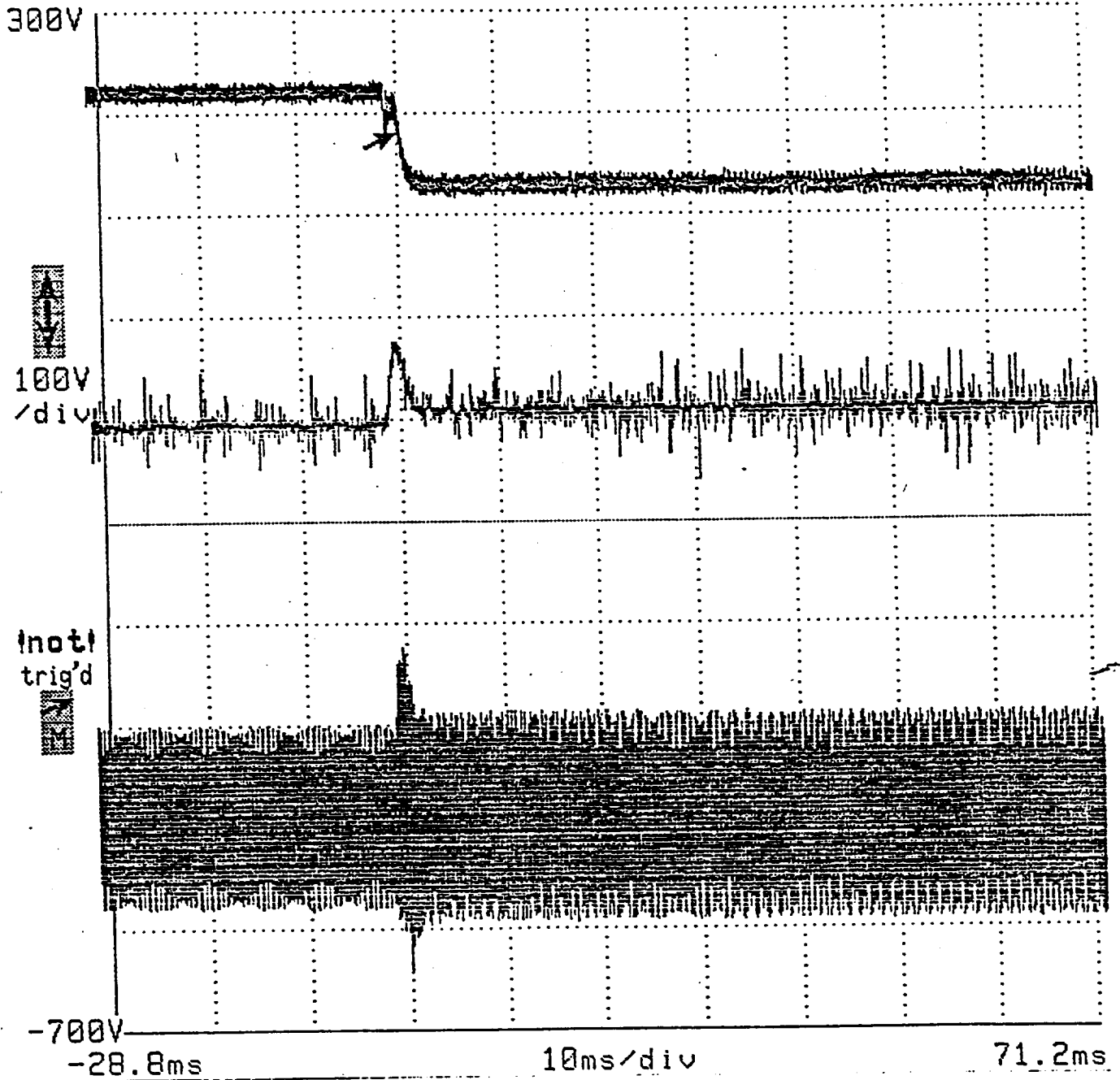


Fig. III-13 Load-resistance step-decrease-transient with initial operation at 220 V, 50 A. Ignition circuit in place.

Upper: Load voltage (100 V/div).

Middle: Load current (50 A/div).

Lower: Resonant tank current (200 A/div).

Timebase: 10 mS/div.

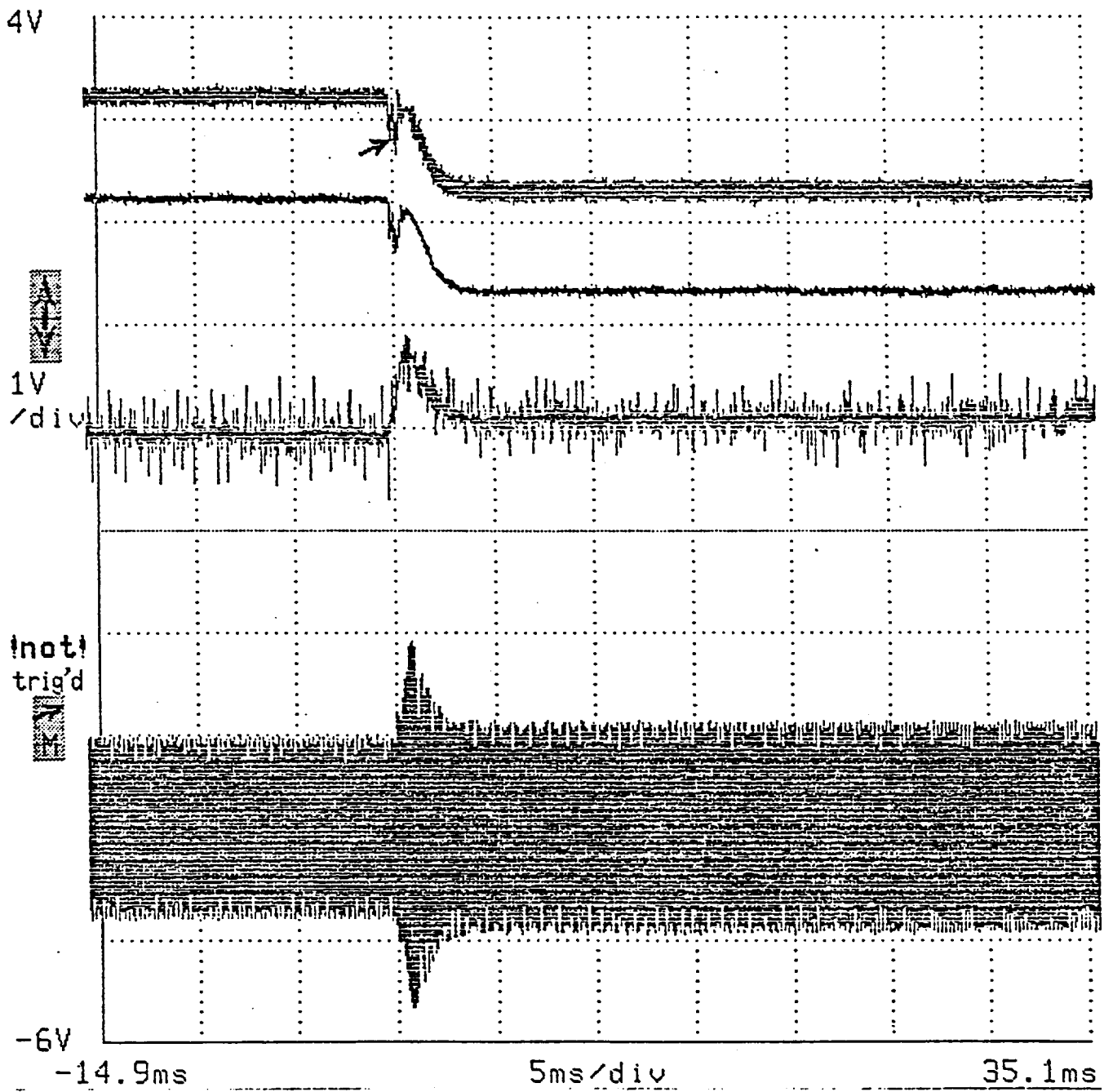


Fig. III-14 Load-resistance step-decrease-transient with initial operation at 220 V, 50 A.
 (Same event as Fig. III-13, ignition circuit in place.)
 Upper: Load voltage (100 V/div).
 Middle: Load current (50 A/div).
 Lower: Resonant tank current (200 A/div).
 Timebase: 5 mS/div.

IV. IGNITION CIRCUIT

A. Power Circuit Design

The power circuit of the arcjet ignitor is shown in Fig. IV-1, and the gate driver is in Fig. IV-2. The design of Fig. IV-1 was motivated by [1]. Closure of the momentary contact switch in the control circuit sets the monostable to gate the IGBT Q1 for a timed pulse of about 24 μ S. Energy is stored in the primary of the coupled inductor L_p , with the IGBT interrupting about 400-500 A of primary current. At turn-off of the IGBT, resonance of L_p/L_s and the IGBT snubber capacitor C1 (1.1 μ F) together with C_{SEC} (0.005 μ F) begins, allowing the IGBT voltage to rise to about 550 V, assuming an open-circuit on the secondary of the ignition circuit. The secondary-side voltage will be ten times this, due to the turns ratio of the coupled inductor. After the IGBT voltage crests, the snubber diode D1 blocks, and resonance continues with L_p/L_s and C_{SEC} only. When the IGBT voltage reaches zero, its anti-parallel diode conducts, allowing recovery of the energy stored in L_p . If the arcjet ignites on the rising edge of the inductor voltage waveform, the energy stored in the inductor at that time establishes the initial current in the arcjet. In either case, some energy is transferred to C1; the 2-K Ω resistor discharges this capacitor. There is an additional monostable in the control which prevents ignition pulses from exceeding a rate of about one per second, thus ensuring reset of the circuit on successive attempts. Winding data for the coupled inductor L_p/L_s are given in Table IV-1.

PRECEDING PAGE BLANK NOT FILMED

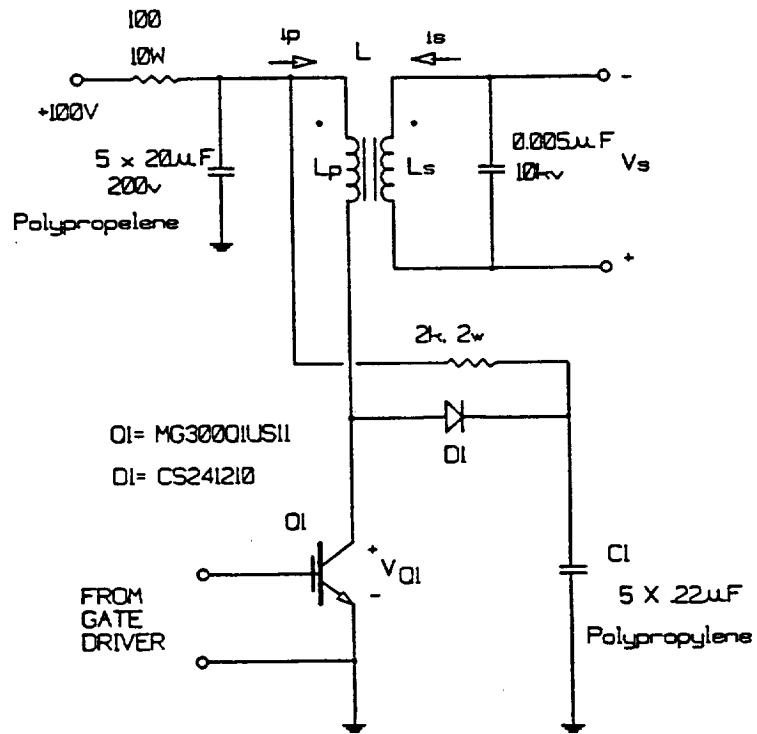


Fig. IV-1 Arcjet ignition power circuit.

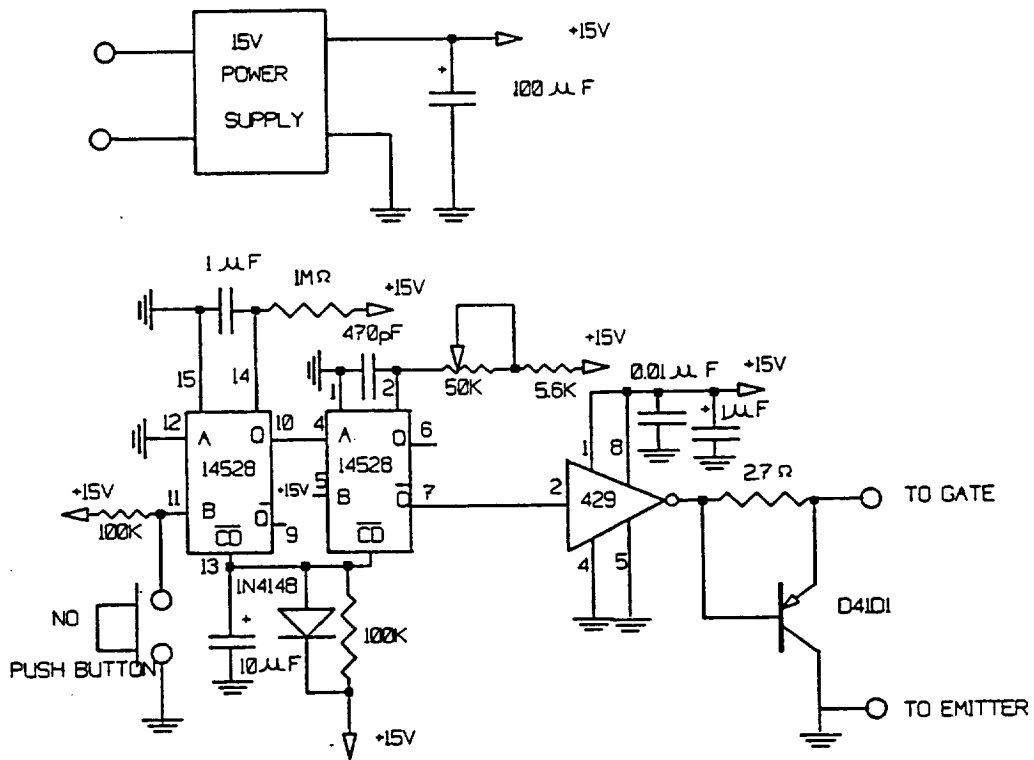


Fig. IV-2 Arcjet ignition gating circuit.

Table IV-1

Winding Data for the Coupled Inductor L_P/L_S

Core:	Powdered iron		Micrometals T520-40D Relative permeability = 60
Primary Winding:	Wound over secondary	$L_P = 2 \mu\text{H}$	2 turns of #14, repeated 20 times, spaced evenly around the circumference of the inductor, and all paralleled.
Secondary Winding:	Wound close to core	$L_S = 200 \mu\text{H}$	20 turns of 4-paralleled #14. Insulated with self-vulcanizing rubber tape

The inductor-charging portion of the ignition pulse is initiated by turn-on of Q1. Energy is transferred from the 100-uF capacitor C_{BYP} to L_P in a resonant fashion. The size of C_{BYP} was limited to bound the collector current that would flow if the IGBT failed to turn off. The period of the inductor-charging resonance is given by:

$$T_{s1} = 2\pi\sqrt{L_P C_{BYP}} = 89 \mu\text{S} \quad (\text{IV-1})$$

The amplitude of the inductor current, primary referred, which could occur if the IGBT failed to turn off is then given by (assuming a 120-V supply):

$$I_{PEAK} = \frac{V_{SUPPLY}}{\sqrt{\frac{L_P}{C_{BYP}}}} = 848 \text{ A} \quad (\text{IV-2})$$

Turn off of Q1 is followed by a rapidly rising inductor voltage as resonance involving the IGBT snubber and secondary-side capacitors occurs. The period of this resonance is given by:

$$T_{S2} = 2\pi\sqrt{L_P C_{EQ}} = 11.2 \mu\text{S}$$

$$\text{where } C_{EQ} = C_1 + C_{SEC} \left(\frac{N_{SEC}}{N_{PRI}} \right)^2 = 1.6 \mu\text{F} \quad (\text{IV-3})$$

The peak value of the voltage, referred to the secondary of the coupled inductor is:

$$V_{\text{PEAK}} = I_{\text{INITIAL}} \sqrt{\frac{L_P}{C_{\text{EQ}}}} \cdot \frac{N_{\text{SEC}}}{N_{\text{PRI}}} = 4.5 \text{ kV} \quad (\text{IV-4})$$

assuming an initial current of 400 A. If the arcjet fails to ignite, this open-circuit voltage will appear on the secondary side of the ignition circuit. The arcjet is expected to break over on the rising portion of this sinusoidal voltage, however. If breakover occurs at the voltage level V_{BO} , then the current transferred to the arc will be:

$$I_{\text{ARC}} = \frac{N_{\text{PRI}}}{N_{\text{SEC}}} I_{\text{INITIAL}} \cos\theta \quad \text{where} \quad \sin\theta = \frac{V_{\text{BO}} \frac{N_{\text{PRI}}}{N_{\text{SEC}}}}{I_{\text{INITIAL}} \sqrt{\frac{L_P}{C_{\text{EQ}}}}} \quad (\text{IV-5})$$

If the arcjet break over is assumed to occur at 1.6 kV, then $\theta = 20.5$ deg and $I_{\text{ARC}} = 37.5$ A. Failure of the arcjet to ignite implies that at the peak of the voltage swing, the IGBT snubber capacitor will be isolated from the resonance by diode D1. The resonance will continue with only the secondary-side capacitor participating. When the IGBT collector voltage reaches zero, its internal anti-parallel diode will conduct, permitting recovery of the energy stored in the coupled inductor back to C_{BYP} .

It is expected that arcjet ignition will occur on the rising part of the inductor voltage waveform, with a substantial portion of the initial stored energy available to establish a secondary current of about 40 A upon arc-over of the arcjet. The closer this secondary current to the current set point in the arcjet power converter, the lesser the magnitude of the transient following ignition, and the less likely a blowout of the arc. Although it was not done here, it may be useful to use a current sense to cause IGBT turn-off at a specific initial current as done in [18]. This current setting could be coordinated with the current set point used in

the power converter; this added feature would be particularly useful if operation with widely varying supply voltage or current set point was expected.

B. Experimental Results

Figs. IV-3 and IV-4 show the experimental waveforms obtained with an open-circuited secondary. (Because these waveforms were obtained as single-event records, sufficient sampling rate was available for only two traces per figure, thus two figures are necessary to record the desired data.) Fig. IV-3 shows the coupled inductor primary current (50 A/div) and IGBT collector voltage (200 V/div) for operation with a 100-V supply and no arcjet. This figure shows a peak IGBT collector current of 400 A, and a peak collector voltage of 550 V. A parasitic resonance involving the leakage inductance associated with the coupled inductor L_p/L_s is evident in the current waveforms. The negative primary current after return of the collector voltage to zero corresponds to the energy-recovery phase of the event. It can also be noted in this figure that the 100- μ F capacitor, initially charged to 100 V, is left with about 40 V at the end of the pulse due to the losses in the circuit. Fig. IV-4 shows the inductor primary current (50 A/div) and secondary voltage (2 kV/div) for the same open-circuit event. The open-circuit secondary voltage is 6 kV.

Figs. IV-5 through IV-8 were obtained using a spark gap to simulate the arcjet, with the gap adjusted to obtain various breakdown voltages. For each of these figures, the secondary voltage v_s is shown at 2 kV/div, and the secondary current is shown at 10 A/div. Table IV-2 records the breakdown voltage V_{BO} observed, along with the current initially established in the arc.

Table IV-2
Breakdown Voltage Versus Initial Arc Current for the
Ignition Circuit

Reference Figure. . .	Breakdown Voltage V_{BO}	Initial Arc Current	Theoretical Breakdown Voltage*
Fig. IV-5	1.0 kV	45 A	1.9 kV
Fig. IV-6	2.5 kV	40 A	2.7 kV
Fig. IV-7	3.5 kV	30 A	3.6 kV
Fig. IV-8	3.8 kV	25 A	3.9 kV

*Based on 500 A initial current at IGBT turn off, and the observed initial arc current

It should be noted that the theoretical calculations are based on a lossless resonance. However, the powdered-iron core and the IGBT forward voltage drop both contribute significant loss to the resonance; therefore there is some discrepancy between the expected and observed voltages and currents. The ignition circuit appears suitable to establish initial currents in the range of 30-40 A in the arcjet, and this can readily be increased to 50 A if necessary by increasing either the IGBT on-time or the size of C_{BYP} .

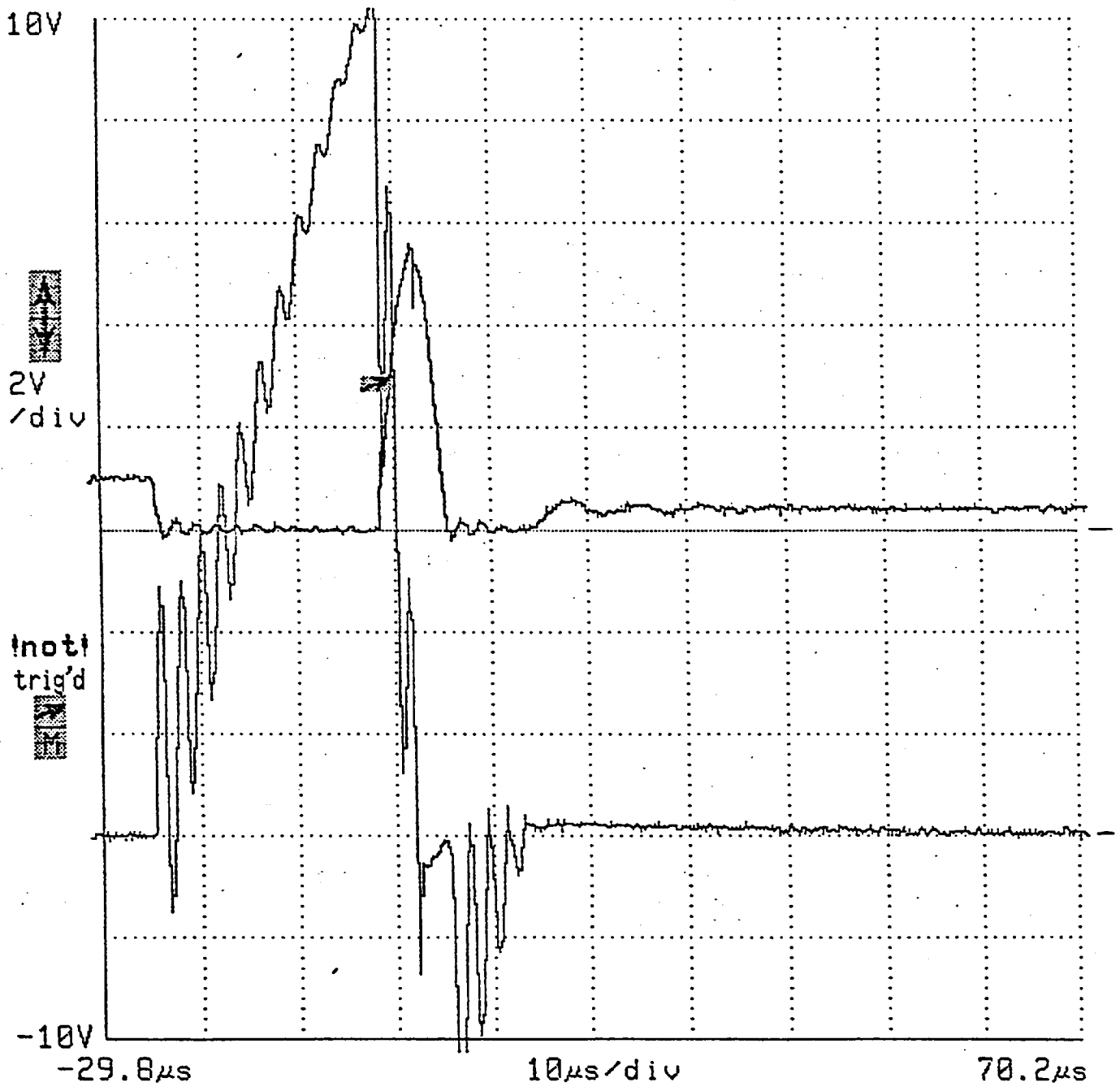


Fig. IV-3 Arcjet ignition circuit waveforms on open-circuit-load.
 Upper: IGBT collector voltage v_{Q1} (200 V/div)
 Lower: Primary current i_p (50 A/div)
 Timebase: 10 μs/div.

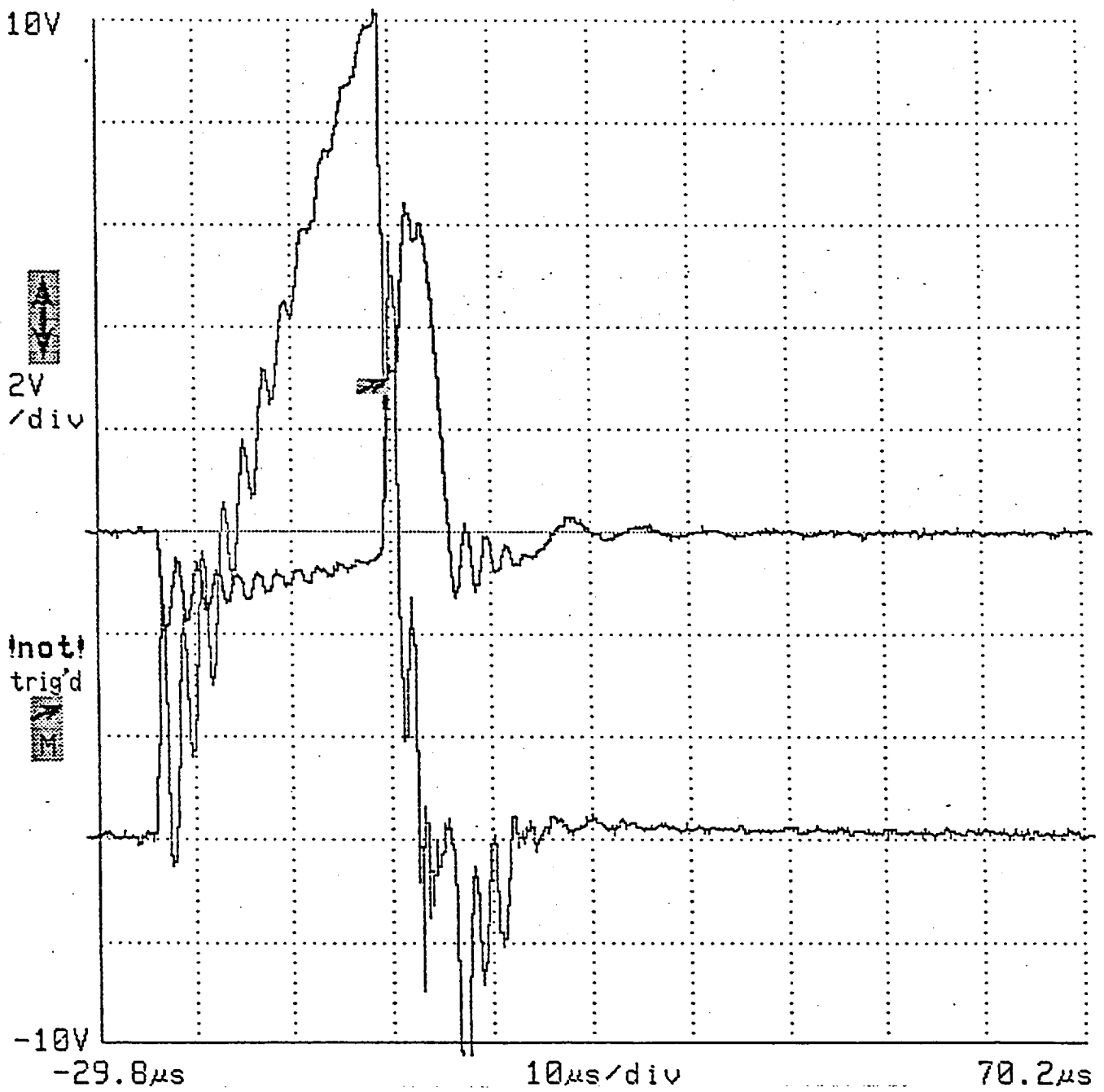


Fig. IV-4 Arcjet ignition circuit waveforms on open-circuit-load.
 Upper: Secondary voltage v_s (2 kV/div)
 Lower: Primary current i_p (50 A/div)
 Timebase: 10 $\mu\text{S}/\text{div}$

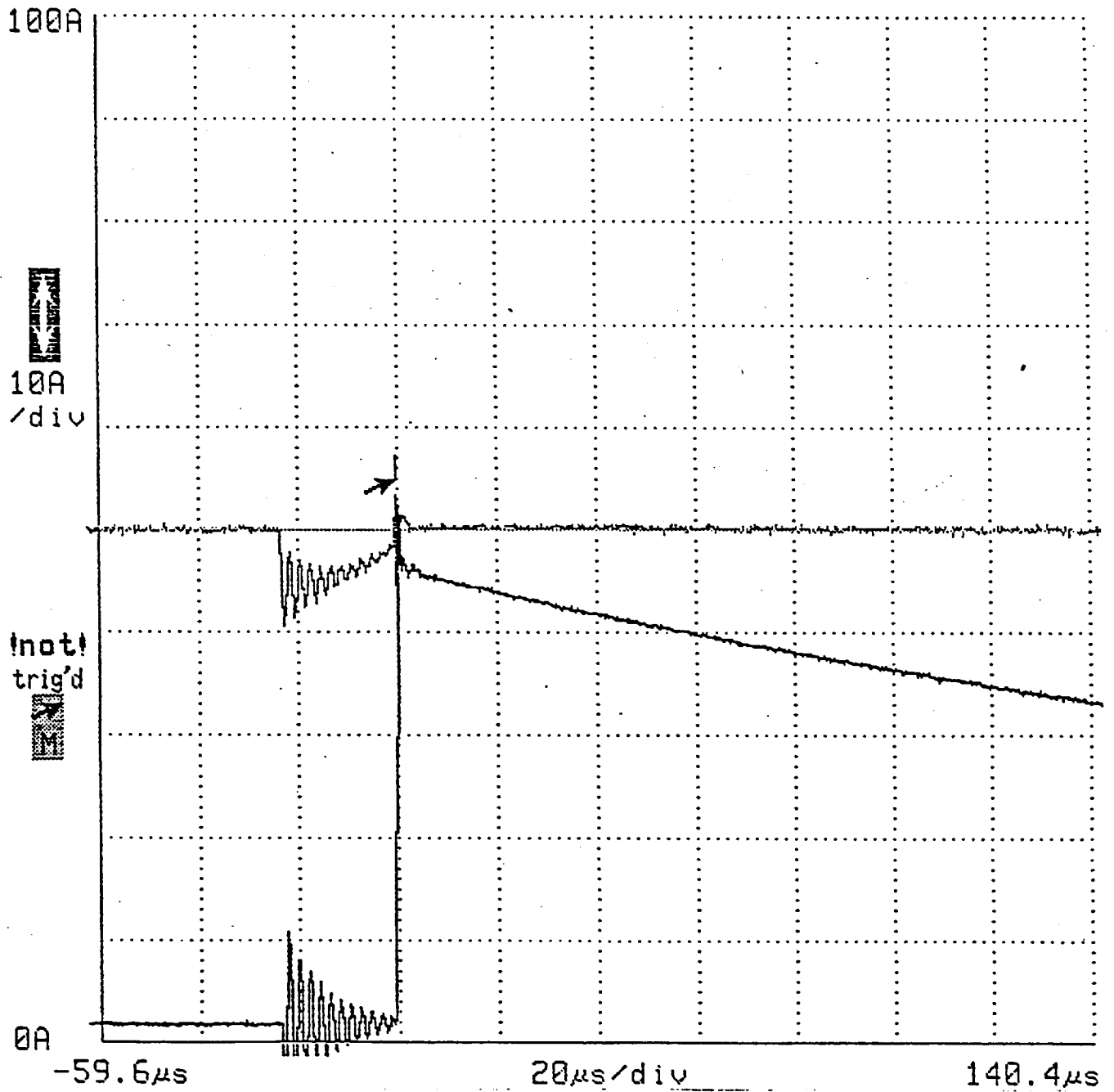


Fig. IV-5 Arcjet ignition circuit waveforms, spark gap adjusted for breakover at 1 kV.
 Upper: Secondary voltage v_s (2 kV/div)
 Lower: Secondary current i_s (10 A/div)
 Timebase: 20 μ S/div.

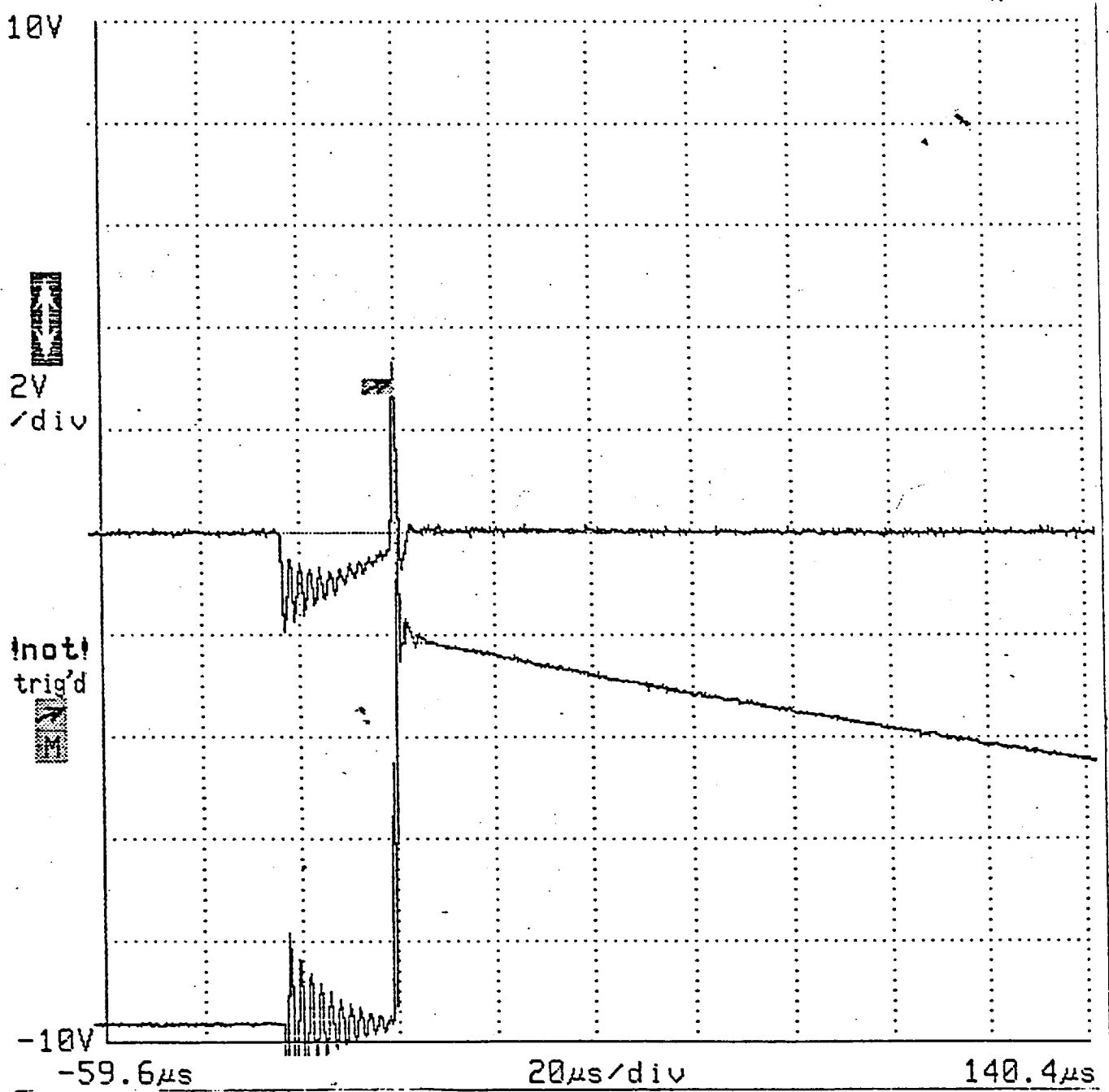


Fig. IV-6 Arcjet ignition circuit waveforms, spark gap adjusted for breakover at 2.5 kV.
 Upper: Secondary voltage v_s (2 kV/div)
 Lower: Secondary current i_s (10 A/div)
 Timebase: 20 μ S/div.

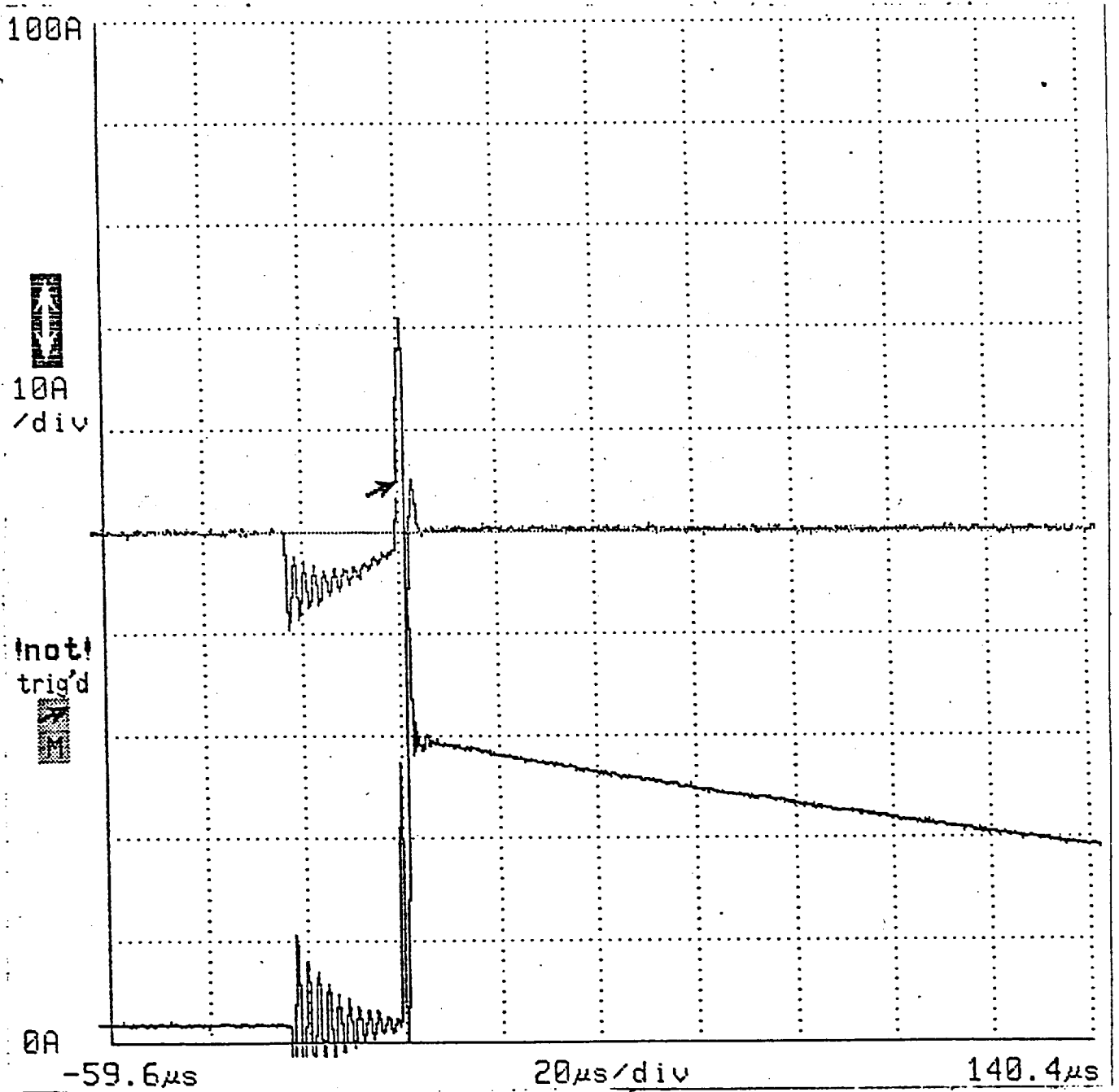


Fig. IV-7 Arcjet ignition circuit waveforms, spark gap adjusted for breakover at 3.5 kV.
 Upper: Secondary voltage v_s (2 kV/div)
 Lower: Secondary current i_s (10 A/div)
 Timebase: 20 μ S/div.

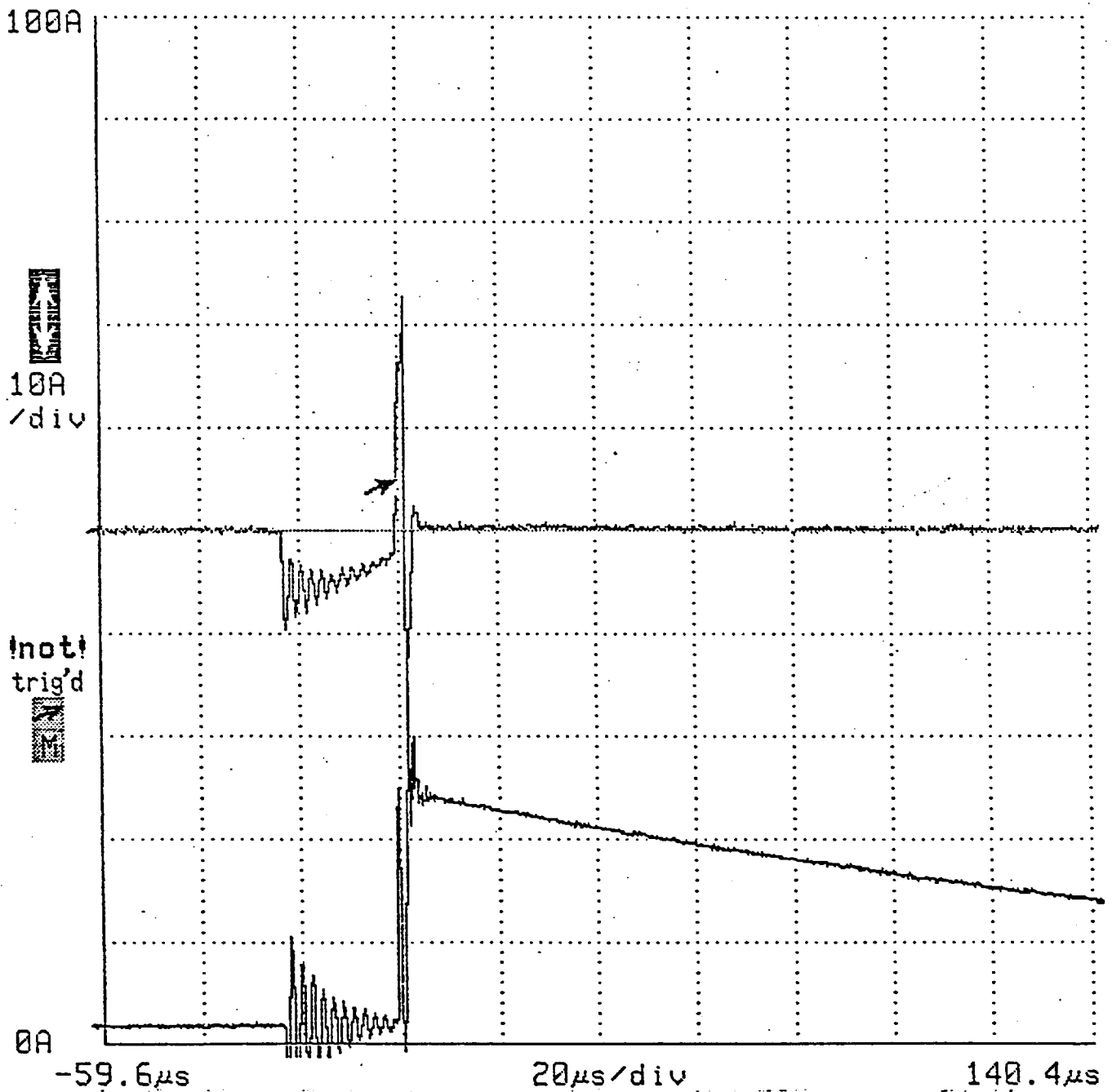


Fig. IV-8 Arcjet ignition circuit waveforms, spark gap adjusted for breakover at 3.8 kV.
 Upper: Secondary voltage v_s (2 kV/div)
 Lower: Secondary current i_s (10 A/div)
 Timebase: 20 μ S/div.

V. SUMMARY

The design of a 10-kW dc/dc converter with a 120-V source has been explored. At this voltage level, the switching device of choice is the MOSFET because of its low switching losses and low conduction losses *if* it is assumed that large numbers of dice can be satisfactorily paralleled. However, at the 10-kW level the number of dice becomes so large that there may be a reliability problem. The use of the MCT as an alternative was therefore chosen for this project. Its high current density at reasonably low conduction losses allowed the use of only three paralleled devices in each switch of the 10-kW full-bridge series-resonant converter.

The series-resonant converter, operating below resonance, was chosen to reduce the turn-off switching loss expected with the MCT. The use of a fast developmental diode (Harris RURU15060) controlled the MCT turn-on losses (and diode turn-off losses). This strategy produced good results with regard to the primary-side switches: The combined switching and conduction losses of the four switching legs was less than 460 W under all conditions. The main difficulty with the series-resonant approach was found to be the resonant inductor, which exhibited losses comparable to those of the switches, reducing the efficiency of the converter. It is believed that further work could significantly improve the design of the inductor, but it remains a large and heavy component.

The overall power efficiency achieved was 91.6% at 10.3 kW output (51.4 A at 201 V). Under this condition, the primary-side switches contributed 407 W out of a total loss of 949 W; the resonant inductor contributed the bulk of the remainder. The power efficiency was generally found to improve at reduced load currents; for example, it was 93.7% at 6.5 kW output (35.7 A at 182.6 V). Under this condition, the primary-side switches contributed the bulk of the loss (348 W out of 441 W).

PRECEDING PAGE BLANK NOT FILMED

The arcjet ignition circuit was readily able to produce open-circuit voltages of 6 kV, and initial currents in the arc in the range 30-40 A. The dependency of the initial arc current on the arc breakdown voltage was predicted theoretically, and confirmed experimentally. Because the arcjet breakdown voltage is not precisely repeatable, there will be some variation in the initial arc current established by the ignition circuit, and thus a current transient following ignition as the arcjet converter's current regulator takes control of the arc current. This is generally a large-signal transient, and is best explored experimentally using either an arcjet, or a load programmed to simulate an arcjet.

Transient testing of the converter using load resistance step changes was done with good results. The converter appears to be readily adapted to stabilizing the arcjet current under start-up and steady-state conditions.

REFERENCES

1. C. J. Sarmiento and R. P. Gruber, "Low Power Arcjet Thruster Pulse Ignition," Proceedings of the AIAA/SAE/ASMA/ASEE 23rd Joint Propulsion Conference, June 29-July 2, 1987, San Diego, CA.
2. J. A. Hamley, "Arcjet Load Characteristics," Proceedings of the AIAA/DGLR/JSASS 21st International Electric Propulsion Conference, July 18-20, 1990, Orlando, FL.
3. T. Stuart, R. King and K. Chen, "An Investigation of Full Bridge DC/DC Converters for Arc Jet Thrusters," Final Report from University of Toledo to NASA Lewis Research Center for Grants NAG3-959 and NAG3-1102, December 1990.
4. R. D. King, A. V. Radun, H. R. Chang and J. A. Rulison, "Comparison of Power Darlington, IGBT and MCT Switching Losses in ASD PWM Inverters," PCIM, pp. 31-40, August 1990.

5. K. Chen and T. Stuart, "The Soft Switch-Avalanche IGBT Converter," IEE Electronics Letters, Vol. 26, No. 19, pp. 1623-1625, September 13, 1990.
6. K. Chen, "A New Zero Current and Zero Voltage Switching Technique Optimized for IGBTs," Ph.D. Dissertation, University of Toledo, Toledo, OH, 1990.
7. K. Chen and T. Stuart, "A 1.6 kW, 110 kHz DC-DC Converter Optimized for IGBTs," IEEE Power Electronics Specialists' Conf. Proc., pp. 139-147, 1991.
8. K. Chen and T. Stuart, "A 1.5 kW, 200 kHz DC-DC Converter Optimized for IGBTs," 1991 High Frequency Power Conversion Conference, Toronto, Canada, 1991.
9. B. Masserant, J. Shriver and T. Stuart, "A 10kW DC-DC Converter Using IGBTs With Active Snubbers," to be published in IEEE Transactions on Aerospace and Electronic Systems, July 1993.
10. F. C. Schwarz, "A Method of Resonant Current Pulse Modulation for Power Converters," IEEE Transactions on Industrial Electronics and Control Instrumentation, IECI-17, pp. 209-221, May 1970.
11. F. C. Schwarz, "An Improved Method of Resonant Current Pulse Modulation for Power Converters," Proceedings of the 1975 IEEE Power Electronics Specialists Conference, pp. 205-215, 1975.
12. F. C. Schwarz and J. B. Klassens, "A 95 percent Efficient 1 kW dc Converter with an Internal Frequency of 50 KHz," IEEE Transactions on Industrial Electronics and Control Instrumentation, IECI-25, pp. 326-333, November 1978.
13. R. King and T. Stuart, "A Normalized Model for the Half Bridge Series Resonant Power Converter," IEEE Transactions in Aerospace and Electronic Systems, Vol. AES-17, pp. 190-198, March 1981.

14. R. King and T. Stuart, "Modelling the Full Bridge Series Resonant Power Converter," IEEE Transactions on Aerospace and Electronic Systems, Vol. AES-18, No. 4, pp. 449-459, July 1982.
15. R. J. King and T. A. Stuart, "Transformer Induced Instability of the Series Resonant Converter," IEEE Trans. on Aerospace and Electron. Sys., Vol. AES-19, pp. 474-482, May 1983.
16. R. King and T. Stuart, "Inherent Overload Protection for the Series Resonant Converter," IEEE Transactions on Aerospace and Electronic Systems, Vol. AES-19, No. 6, pp. 820-830, November 1983.
17. R. R. Robson, "25-Kilowatt Series Resonant DC/DC Power Converter," NASA Contract Report, CR-168273, Jan. 1984.
18. T. A. Stuart, R. J. King and G. P. Altenburger, "A Study of Ignition and Simulation Circuits for Arcjet Thrusters," Final report from University of Toledo to NASA Lewis Research Center for Grant NAG3-1102, December 1991.

REPORT DOCUMENTATION PAGEForm Approved
OMB No. 0704-0188

Public reporting burden for this collection of information is estimated to average 1 hour per response, including the time for reviewing instructions, searching existing data sources, gathering and maintaining the data needed, and completing and reviewing the collection of information. Send comments regarding this burden estimate or any other aspect of this collection of information, including suggestions for reducing this burden, to Washington Headquarters Services, Directorate for Information Operations and Reports, 1215 Jefferson Davis Highway, Suite 1204, Arlington, VA 22202-4302, and to the Office of Management and Budget, Paperwork Reduction Project (0704-0188), Washington, DC 20503.

1. AGENCY USE ONLY (Leave blank)		2. REPORT DATE January 1994	3. REPORT TYPE AND DATES COVERED Final Contractor Report	
4. TITLE AND SUBTITLE A Study of DC-DC Converters With MCT's for Arcjet Power Supplies			5. FUNDING NUMBERS WU-506-42-31 G-NAG3-1102	
6. AUTHOR(S) Thomas A. Stuart				
7. PERFORMING ORGANIZATION NAME(S) AND ADDRESS(ES) University of Toledo 2801 W. Bancroft Street Toledo, Ohio 43606			8. PERFORMING ORGANIZATION REPORT NUMBER E-8386	
9. SPONSORING/MONITORING AGENCY NAME(S) AND ADDRESS(ES) National Aeronautics and Space Administration Lewis Research Center Cleveland, Ohio 44135-3191			10. SPONSORING/MONITORING AGENCY REPORT NUMBER NASA CR-191204	
11. SUPPLEMENTARY NOTES Project Manager, John A. Hamley, Space Propulsion Technology Division, organization code 5330, NASA Lewis Research Center, (216) 977-7430.				
12a. DISTRIBUTION/AVAILABILITY STATEMENT Unclassified - Unlimited Subject Category 20			12b. DISTRIBUTION CODE	
13. ABSTRACT (Maximum 200 words) Many arcjet DC power supplies use PWM full bridge converters with large arrays of parallel FETs. This report investigates an alternative supply using a variable frequency series resonant converter with small arrays of parallel MCTs. The reasons for this approach are to: 1) Increase reliability by reducing the number of switching devices; 2) Decrease the surface mounting area of the switching arrays. The variable frequency series resonant approach is used because the relatively slow switching speed of the MCT precludes the use of PWM. The 10kW converter operated satisfactorily with an efficiency of over 91%. Test results indicate this efficiency could be increased further by additional optimization of the series resonant inductor.				
14. SUBJECT TERMS Electric propulsion; Power processing; Arcjet thruster			15. NUMBER OF PAGES 80	
			16. PRICE CODE A04	
17. SECURITY CLASSIFICATION OF REPORT Unclassified	18. SECURITY CLASSIFICATION OF THIS PAGE Unclassified	19. SECURITY CLASSIFICATION OF ABSTRACT Unclassified	20. LIMITATION OF ABSTRACT	